



**COMPLEX BIFURCATIONS AND NOISE-INDUCED
TRANSITIONS: A PREDATION MODEL WITH FEAR EFFECT
IN PREY AND CROWDING EFFECT IN PREDATORS**

CUIHUA WANG^{✉1}, HAO WANG^{✉2} AND SANLING YUAN^{✉*1}

¹University of Shanghai for Science and Technology
Shanghai 200093, China

²Department of Mathematical and Statistical Sciences
University of Alberta
Edmonton, AB T6G2G1, Canada

(Communicated by Dongmei Xiao)

ABSTRACT. It has been well established in the literature that the predator-induced fear has indirect impact on prey but can have comparable effects on prey population as direct killing, and that the crowding effect or self-limitation of population plays pivotal roles in determining the dynamics and interactions among populations. In this paper, we first propose and investigate a deterministic prey-predator model incorporating simultaneously fear effect in prey and crowding effect in predators. The model has rich dynamics, including one up to three positive equilibria, complex bifurcations (saddle-node, Hopf and Bogdanov-Takens bifurcations), and two types of bistability (between two interior equilibria or between an interior equilibrium and an interior limit cycle). Thus the model is easily affected by external environmental fluctuations. When environmental noises are involved, some new dynamics can be observed for the developed stochastic model. Especially, for the scenarios when the deterministic model exhibits bistability, we can observe noise-induced frequent transitions between two different interior attractors (two interior equilibria or an interior equilibrium and an interior limit cycle). The tipping points of noise intensities for the occurrence of such transitions are estimated by constructing the confidence ellipse/band for the equilibrium/limit cycle. These indicate that the predators and prey can coexist in two different modes and switch randomly between them.

1. Introduction. To understand species' interactions and their impacts on the persistence and biodiversity of an ecosystem is a central question in ecology [3, 36]. There are many types of interactions between species such as predation, competition, mutualism and so on, among which predation is one of the most important ecological processes. Through predation animals capture prey and obtain energy to support their survival and reproduction. On the other hand, prey faces the risk of predation at any time and thus has various anti-predator behaviors such as habitat change, increased vigilance, reduced foraging, increased group defense [6]. This predation risk effect (also called fear effect) is common and can be as strong

2020 *Mathematics Subject Classification.* Primary: 92-10, 34C23.

Key words and phrases. Predator-induced fear, Crowding effect, Prey-predator model, Bifurcation, Stochastic sensitivity analysis, Confidence domains.

*Corresponding author: Sanling Yuan.

as or sometimes greater than direct killing as recent empirical studies have shown [4, 13, 16, 18, 32].

In most situations, the fear effect is inevitable, but it is usually ignored in classical predator-prey models [31, 35]. If the predator-induced fear on prey is ignored in an intimidating environment, there will be a large deviation in the prediction of population ecology [12, 33]. Recently, many studies qualitatively explored the indirect impact of predation on populations and then evaluated the real impact of predation induced fear effect [5, 7, 11, 14, 19, 21, 25, 26, 27, 28, 34]. Wang et al. formulated a mathematical model by introducing a fear function to describe the decrease of the birth rate of prey caused by indirect predation [26]. This modeling approach provides a good framework for further understanding the effects of fear on populations. For example, Wang et al. further considered the benefits of anti-predation behaviors and digestion delay. They found that if the predation function is described by Holling-II functional response function, moderate fear and large digestion delay can induce the occurrence of periodic oscillations [28]. Considering the fact that the predation risk can also increase the death rate of prey, Das et al. investigated a predator-prey model with this risk effect as well as the intraspecific competition in predators, indicating that a higher degree of fear or intraspecific competition is conducive to species coexistence [7]. In another paper [14], Pal et al. developed a Leslie-Gower type model with fear effect and cooperative predation, indicating that the fear can exclude the existence of periodic oscillations such that the predator-prey system eventually approaches a steady state, and moreover the system with only fear effect is more robust than that with only hunting cooperation. In [9], Hossain et al. investigated an intraguild predation model with fear effect, revealing that fear can stabilize the model by period-halving bifurcation. All these studies demonstrate that fear does play a significant role in assessing the total impact of predation on populations.

As indicated in [8], to achieve the plausible model behaviour, suitable mortality terms should be considered for different populations. It has now been well established in the literature that the linear mortality is enough for top predators, however, for some predators, especially for intermediate predators (for example, piscivores), the quadratic mortality is a reasonable choice [8, 20] because the crowding effect (or self-limitation) of intermediate predators dominates their natural mortality [24]. Intermediate predators play pivotal roles in the transition of elements and energy in an ecosystem. However, as far as we know, few efforts have been devoted to the investigation of a fearful predator-prey model with self-limitation in predators. This paper aims to explore this issue by considering the following prey-predator model:

$$\begin{aligned}\frac{du}{dt} &= \frac{ru}{1+kv} - du - au^2 - \frac{puv}{1+cu}, \\ \frac{dv}{dt} &= -mv^2 + \frac{quv}{1+cu},\end{aligned}\tag{1}$$

where r and d stand respectively for the prey growth rate and the natural death rate in the absence of fear and predators. The parameter a is the prey density-dependent mortality rate measuring the prey intra-specific competition, and m is the crowding effect parameter for predators. The function $\frac{1}{1+kv}$ describes the fear cost of predation, where k denotes the fear level. The predation is described by a Holling-II type functional response function, where p and q are respectively the predation rate and growth rate of predators, and $\frac{1}{c}$ is the half saturation constant. Our analysis shows that the fear caused by predators and the self-limitation in predators can

make the model exhibit rich dynamics such as complex bifurcations and bistability phenomena, and just because of these the model is sensitive to and easily affected by external environmental fluctuations which always exist in the real world. Especially, for the scenarios when the deterministic model exhibits bistability, we numerically estimate the tipping points of noise intensities for the occurrence of such switching by constructing the confidence ellipse (confidence band) for the equilibrium (the limit cycle).

The organization of this paper is as follows. The existence and stability of the equilibria of model (1) are discussed in the next section. The detailed analysis of possible bifurcations for model (1), including saddle-node bifurcation, Hopf bifurcation and Bogdanov-Takens bifurcation are performed in Section 3. In order to verify and illustrate the mathematical results, in Section 4, we present the one-parameter and two-parameter bifurcation diagrams and phase plane diagrams of model (1) to display the influence of the predator-induced fear and predators' crowding effect parameter on the population dynamics. To further illustrate how the environmental noises affect the dynamics of the model, especially in the scenario that the model exhibits bistability, we proceed to study in Section 5 the possible noise-induced transitions between different stochastic attractors and numerically estimate the critical values of noise intensity for the occurrence of such transition with the aids of the technique of stochastic sensitivity functions. Finally, we provide some concluding remarks in Section 6.

2. Existence and stability of equilibria. By the biological meanings of prey and the predators, we only pay our attention to model (1) in $\mathbb{R}_+^2 = \{(u, v) | u \geq 0, v \geq 0\}$. The positivity and boundedness of solutions of model (1) are guaranteed by the following theorem.

Theorem 2.1. *For any given nonnegative initial value $(u(0), v(0)) \in \mathbb{R}_+^2$, the solution $(u(t), v(t))$ of model (1) is positive and uniformly ultimately bounded for all $t \geq 0$.*

Proof. Notice that $u = 0$ and $v = 0$ are both solutions of model (1). The positivity of the solution follows directly from the existence and uniqueness theorem of solutions for ordinary differential equations (ODE). Denote $w = qu + pv$, then we have

$$\begin{aligned} \frac{dw}{dt} &= \frac{rqu}{1 + kv} - dqu - aqu^2 - pmv^2 \\ &\leq -d(qu + pv) + dpv + rqu - aqu^2 - pmv^2 \\ &\leq -dw + \frac{r^2q}{4a} + \frac{d^2p}{4m}, \end{aligned} \quad (2)$$

which implies that $\limsup_{t \rightarrow \infty} w(t) \leq \frac{r^2q}{4ad} + \frac{dp}{4m}$. In addition, from the first equation of (1), we can easily obtain that $\limsup_{t \rightarrow \infty} u(t) \leq \frac{r-d}{a}$. Thus any solution of model (1) with nonnegative values will tend to or stay forever in the region

$$\Omega = \left\{ (u, v) \mid 0 \leq u \leq \frac{r-d}{a}, 0 \leq qu + pv \leq \frac{r^2q}{4ad} + \frac{d^2p}{4md} \right\}. \quad (3)$$

The proof is thus completed. \square

We now study the existence and stability of equilibria of model (1). From Theorem 1 in [23], one can know that when $r \leq d$, there only exists a trivial equilibrium

$E^0(0, 0)$ and it is globally asymptotically stable; when $r > d$, $E^0(0, 0)$ becomes unstable and a semi-trivial equilibrium $E^1(\frac{r-d}{a}, 0)$ emerges, which is always a saddle point. For the positive equilibrium, it has been shown in [23] that model (1) has at least one if $r > d$. Here, we will further show model (1) has at most three positive equilibria.

Any positive equilibrium $E^*(u^*, v^*)$ of model (1), if it exists, must satisfy $v^* = \frac{qu^*}{m(1+cu^*)}$, where u^* is a positive root of $h(u) := f(u) - g(u) = 0$, where

$$f(u) = \frac{rm(1+cu)}{m+(cm+kq)u}, \quad g(u) = d+au + \frac{pqu}{m(1+cu)^2}. \quad (4)$$

The equation $h(u) = 0$ can be rewritten as

$$F(u) := \ell_4 u^4 + \ell_3 u^3 + \ell_2 u^2 + \ell_1 u + \ell_0 = 0, \quad (5)$$

where

$$\begin{aligned} \ell_4 &= ac^2m(mc+kq) > 0, \\ \ell_3 &= cm(cd+2a)(mc+kq) + c^2m^2(a-cr), \\ \ell_2 &= (am+2cdm+pq)(mc+kq) + cm^2(cd+2a) - 3c^2rm^2, \\ \ell_1 &= dm(mc+kq) + m(am+2cdm+pq) - 3crm^2, \\ \ell_0 &= (d-r)m^2 < 0. \end{aligned} \quad (6)$$

Therefore, it suffices to discuss the existence and number of the positive roots of $F(u) = 0$. The details are provided in Appendix A. Define $F_1(u) = F'(u)$ and $F_2(u) = F''(u)$, that is,

$$F_1(u) = 4\ell_4 u^3 + 3\ell_3 u^2 + 2\ell_2 u + \ell_1, \quad F_2(u) = 12\ell_4 u^2 + 6\ell_3 u + 2\ell_2.$$

The following theorem is about the existence of equilibria of model (1).

Theorem 2.2. *Model (1) always has a trivial equilibrium $E^0(0, 0)$, which is unique provided $r \leq d$. When $r > d$, model (1) also possesses a semi-trivial equilibrium $E^1(\frac{r-d}{a}, 0)$, and at least one positive equilibrium and at most three positive equilibria. More specifically,*

(1) if $\ell_3^2 \leq \frac{8}{3}\ell_2\ell_4$, model (1) has a unique positive equilibrium $E^*(u^*, v^*)$.

(2) if $\ell_3^2 > \frac{8}{3}\ell_2\ell_4$ and

(2a) $\ell_2 < 0$ or $\ell_2 = 0$, $\ell_3 < 0$, then when $\ell_1 \leq 0$, model (1) has a unique positive equilibrium $E^*(u^*, v^*)$; while

(2a-1) when $\ell_1 > 0$ and $F_1(\beta_2) > 0$, model (1) has a unique positive equilibrium $E^*(u^*, v^*)$.

(2a-2) when $\ell_1 > 0$ and $F_1(\beta_2) = 0$, if further $F(\beta_2) = 0$, then model (1) has a positive equilibrium $(\beta_2, \frac{q\beta_2}{m(1+c\beta_2)})$ with multiplicity 3; otherwise model (1) has a unique positive equilibrium $E^*(u^*, v^*)$.

(2a-3) when $\ell_1 > 0$ and $F_1(\beta_2) < 0$, if $F(\gamma_1) > 0$ and $F(\gamma_2) < 0$, model (1) has three positive equilibria $E_1^*(u_1^*, v_1^*)$, $E_2^*(u_2^*, v_2^*)$ and $E_3^*(u_3^*, v_3^*)$ with $u_1^* < u_2^* < u_3^*$; if $F(\gamma_1) = 0$, $E_1^*(u_1^*, v_1^*)$ and $E_2^*(u_2^*, v_2^*)$ coincide into an equilibrium $E_{1,2}^*(u_{1,2}^*, v_{1,2}^*)$, and then the model has two positive equilibria $E_{1,2}^*(u_{1,2}^*, v_{1,2}^*)$ and $E_3^*(u_3^*, v_3^*)$ with $u_{1,2}^* < u_3^*$; if $F(\gamma_1) < 0$, $E_{1,2}^*(u_{1,2}^*, v_{1,2}^*)$ disappears and the model has a unique positive equilibrium $E_3^*(u_3^*, v_3^*)$; if $F(\gamma_2) = 0$, $E_2^*(u_2^*, v_2^*)$ and $E_3^*(u_3^*, v_3^*)$ coincide into an equilibrium $E_{2,3}^*(u_{2,3}^*, v_{2,3}^*)$, and then the model has two positive equilibria $E_1^*(u_1^*, v_1^*)$ and $E_{2,3}^*(u_{2,3}^*, v_{2,3}^*)$ with $u_1^* < u_{2,3}^*$;

- if $F(\gamma_2) > 0$, $E_{2,3}^*(u_{2,3}^*, v_{2,3}^*)$ disappears and the model has a unique positive equilibrium $E_1^*(u_1^*, v_1^*)$.
- (2b) $\ell_2 \geq 0$, $\ell_3 \geq 0$, then model (1) has a unique positive equilibrium $E^*(u^*, v^*)$.
- (2c) $\ell_2 > 0$, $\ell_3 < 0$, then
- (2c-1) when $\ell_1 < 0$, $F_1(\beta_1) \leq 0$ or $F_1(\beta_2) \geq 0$, then $F(u) = 0$ has a unique positive equilibrium $E^*(u^*, v^*)$.
- (2c-2) when $\ell_1 < 0$, $F_1(\beta_1) > 0$ and $F_1(\beta_2) < 0$, if $F(\gamma_2) > 0$ and $F(\gamma_3) < 0$, then model (1) has three positive equilibria $E_1^*(u_1^*, v_1^*)$, $E_2^*(u_2^*, v_2^*)$ and $E_3^*(u_3^*, v_3^*)$ with $u_1^* < u_2^* < u_3^*$; if $F(\gamma_2) = 0$, $E_1^*(u_1^*, v_1^*)$ and $E_2^*(u_2^*, v_2^*)$ coincide into an equilibrium $E_{1,2}^*(u_{1,2}^*, v_{1,2}^*)$, and then model has two positive equilibria $E_{1,2}^*(u_{1,2}^*, v_{1,2}^*)$ and $E_3^*(u_3^*, v_3^*)$ with $u_{1,2}^* < u_3^*$; if $F(\gamma_2) < 0$, $E_{1,2}^*(u_{1,2}^*, v_{1,2}^*)$ disappears and the model has a unique positive equilibrium $E_3^*(u_3^*, v_3^*)$; if $F(\gamma_3) = 0$, $E_2^*(u_2^*, v_2^*)$ and $E_3^*(u_3^*, v_3^*)$ coincide into an equilibrium $E_{2,3}^*(u_{2,3}^*, v_{2,3}^*)$ and then the model has two positive equilibria $E_1^*(u_1^*, v_1^*)$ and $E_{2,3}^*(u_{2,3}^*, v_{2,3}^*)$ with $u_1^* < u_{2,3}^*$; if $F(\gamma_3) > 0$, $E_{2,3}^*(u_{2,3}^*, v_{2,3}^*)$ disappears and the model has a unique positive equilibrium $E_1^*(u_1^*, v_1^*)$.
- (2c-3) when $\ell_1 \geq 0$, $F_1(\beta_2) > 0$, then model (1) has a unique positive equilibrium $E^*(u^*, v^*)$.
- (2c-4) when $\ell_1 \geq 0$, $F_1(\beta_2) = 0$, if further $F(\beta_2) = 0$, then model (1) has a positive equilibrium $(\beta_2, \frac{q\beta_2}{m(1+c\beta_2)})$ with multiplicity 3; otherwise model (1) has a unique positive equilibrium $E^*(u^*, v^*)$.
- (2c-5) when $\ell_1 \geq 0$, $F_1(\beta_2) < 0$, if $F(\gamma_1) > 0$ and $F(\gamma_2) < 0$, then model (1) has three positive equilibria $E_1^*(u_1^*, v_1^*)$, $E_2^*(u_2^*, v_2^*)$ and $E_3^*(u_3^*, v_3^*)$ with $u_1^* < u_2^* < u_3^*$; if $F(\gamma_1) = 0$, $E_1^*(u_1^*, v_1^*)$ and $E_2^*(u_2^*, v_2^*)$ coincide into an equilibrium $E_{1,2}^*(u_{1,2}^*, v_{1,2}^*)$, and then the model has two positive equilibria $E_{1,2}^*(u_{1,2}^*, v_{1,2}^*)$ and $E_3^*(u_3^*, v_3^*)$ with $u_{1,2}^* < u_3^*$; if $F(\gamma_1) < 0$, $E_{1,2}^*(u_{1,2}^*, v_{1,2}^*)$ disappears and the model has a unique positive equilibrium $E_3^*(u_3^*, v_3^*)$; if $F(\gamma_2) = 0$, $E_2^*(u_2^*, v_2^*)$ and $E_3^*(u_3^*, v_3^*)$ coincide into an equilibrium $E_{2,3}^*(u_{2,3}^*, v_{2,3}^*)$ and then the model has two positive equilibria $E_1^*(u_1^*, v_1^*)$ and $E_{2,3}^*(u_{2,3}^*, v_{2,3}^*)$ with $u_1^* < u_{2,3}^*$; if $F(\gamma_2) > 0$, $E_{2,3}^*(u_{2,3}^*, v_{2,3}^*)$ disappears and the model has a unique positive equilibrium $E_1^*(u_1^*, v_1^*)$.

Here β_i ($i = 1, 2$) are the roots of $F_2(u) = 0$; γ_i ($i = 1, 2, 3$) are the roots of $F_1(u) = 0$.

The Jacobi matrix of model (1) at any positive equilibrium $E^*(u^*, v^*)$ has the form

$$J(E^*) = \begin{pmatrix} \frac{r}{1+kv^*} - d - 2au^* - \frac{pv^*}{(1+cu^*)^2} & -\left(\frac{kru^*}{(1+kv^*)^2} + \frac{pu^*}{1+cu^*}\right) \\ \frac{qu^*}{(1+cu^*)^2} & \frac{qu^*}{1+cu^*} - 2mv^* \end{pmatrix} := \begin{pmatrix} J_{11} & J_{12} \\ J_{21} & J_{22} \end{pmatrix}. \quad (7)$$

Then the corresponding characteristic equation is

$$\lambda^2 - \varphi(u^*)\lambda + \psi(u^*) = 0, \quad (8)$$

where

$$\varphi(u^*) = -au^* + \frac{qu^*}{1+cu^*} \left(\frac{cpu^*}{m(1+cu^*)^2} - 1 \right), \quad (9)$$

$$\psi(u^*) = -\frac{qu^{*2}}{1+cu^*} h'(u^*). \quad (10)$$

It then follows from the stability theory that $E^*(u^*, v^*)$ is stable if $h'(u^*) < 0$ and $\varphi(u^*) < 0$ and unstable if $h'(u^*) > 0$ or $\varphi(u^*) > 0$.

To summarize, we obtain the following stability result of model (1).

Theorem 2.3. *For the equilibria of model (1), we have*

- (1) $E^0(0, 0)$ is globally attractive for $r \leq d$ and unstable for $r > d$.
- (2) $E^1(\frac{r-d}{a}, 0)$ is always a saddle provided it exists (i.e., $r > d$).
- (3) Any positive equilibrium $E^*(u^*, v^*)$ of model (1), when exists, is stable provided $h'(u^*) < 0$ and $\varphi(u^*) < 0$, and unstable provided $h'(u^*) > 0$ or $\varphi(u^*) > 0$.

3. Bifurcation analysis. From Theorem 2.3, we know that a degenerate positive equilibrium $E^*(u^*, v^*)$ emerges if u^* further satisfies $F_1(u^*) = 0$, i.e., $h'(u^*) = 0$. In this case, the characteristic equation (8) has one or two zero roots and then model (1) may undergo some complicated bifurcations such as saddle-node bifurcation, Hopf bifurcation, and Bogdanov-Takens bifurcation.

3.1. Saddle-node bifurcation.

Theorem 3.1. *Suppose that $r > d$ and $E^*(u^*, v^*)$ is a positive equilibrium of model (1). If $\ell_3^2 > \frac{8}{3}\ell_2\ell_4$, $F_1(u^*) = 0$, $F_2(u^*) \neq 0$ and $\varphi(u^*) \neq 0$, then model (1) undergoes a saddle-node bifurcation at $E^*(u^*, v^*)$.*

Proof. If $F_1(u^*) = 0$, then $h'(u^*) = 0$ and we can directly obtain that $\psi(u^*) = 0$. In this situation, the roots of characteristic equation (8) at the equilibrium $E^*(u^*, v^*)$ are 0 and $-au^* + \frac{qu^*}{1+cu^*} \left(\frac{cpu^*}{m(1+cu^*)^2} - 1 \right)$. To derive the normal form of model (1), we firstly transform $E^*(u^*, v^*)$ into the origin by the linear translation $\tilde{u} = u - u^*$ and $\tilde{v} = v - v^*$, then model (1) becomes

$$\begin{aligned} \frac{d\tilde{u}}{dt} &= a_{10}\tilde{u} + a_{01}\tilde{v} + \sum_{2 \leq i+j \leq 3} a_{ij}\tilde{u}^i\tilde{v}^j + \mathcal{O}(|\tilde{u}, \tilde{v}|^4), \\ \frac{d\tilde{v}}{dt} &= b_{10}\tilde{u} + b_{01}\tilde{v} + \sum_{2 \leq i+j \leq 3} b_{ij}\tilde{u}^i\tilde{v}^j + \mathcal{O}(|\tilde{u}, \tilde{v}|^4), \end{aligned} \quad (11)$$

where

$$\begin{aligned} a_{10} &= -au^* + \frac{cpqu^{*2}}{m(1+cu^*)^3}, \quad a_{01} = -\frac{krm^2u^*(1+cu^*)^2}{(m+(mc+kq)u^*)^2} - \frac{pu^*}{1+cu^*}, \\ a_{11} &= \frac{-krm^2(1+cu^*)^2}{(m+(mc+kq)u^*)^2} - \frac{p}{(1+cu^*)^2}, \quad a_{20} = -a + \frac{cpqu^*}{m(1+cu^*)^4}, \\ a_{02} &= \frac{k^2rm^3u^*(1+cu^*)^3}{(m+(mc+kq)u^*)^3}, \quad a_{21} = \frac{cp}{(1+cu^*)^3}, \quad a_{12} = \frac{k^2rm^3(1+cu^*)^3}{(m+(mc+kq)u^*)^3}, \\ a_{30} &= \frac{-c^2pqu^*}{m(1+cu^*)^5}, \quad a_{03} = \frac{-k^3rm^4u^*(1+cu^*)^4}{(m+(mc+kq)u^*)^4}, \quad b_{11} = \frac{q}{(1+cu^*)^2}, \\ b_{20} &= \frac{-cq^2u^*}{m(1+cu^*)^4}, \quad b_{10} = \frac{q^2u^*}{m(1+cu^*)^3}, \quad b_{01} = -\frac{qu^*}{1+cu^*}, \\ b_{02} &= -m, \quad b_{21} = \frac{-cq}{(1+cu^*)^3}, \quad b_{30} = \frac{c^2q^2u^*}{m(1+cu^*)^5}, \quad b_{12} = b_{03} = 0. \end{aligned}$$

By making the linear transformation

$$\tilde{u} = - \left(\frac{qu^*}{1+cu^*} - 2mv^* \right) U + \left(\frac{r}{1+kv^*} - d - 2au^* - \frac{pv^*}{(1+cu^*)^2} \right) V$$

and

$$\tilde{v} = \frac{qv^*}{(1+cu^*)^2} (U + V),$$

we obtain

$$\begin{aligned} \frac{dU}{dt} &= - \frac{(l_1 U^2 + l_2 UV + l_3 V^2) + O(|U, V|^3)}{b_{10}(a_{10} + b_{01})}, \\ \frac{dV}{dt} &= (a_{10} + b_{01})V + O(|U, V|^2), \end{aligned} \quad (12)$$

where

$$\begin{aligned} l_1 &= \frac{q^4 u^{*4}}{m(1+cu^*)^5} \left(\frac{2cpq(2-cu^*)}{m(1+cu^*)^4} + \frac{2krmq(cm+kq)}{(m+(cm+kq)u^*)^3} \right) \\ &= \frac{q^4 u^{*4}}{m(1+cu^*)^5} h''(u^*). \end{aligned}$$

Since $F_2(u^*) \neq 0$ and $\varphi(u^*) \neq 0$, we have $h''(u^*) \neq 0$ and then $l_1 \neq 0$. According to the center manifold theory, we know that for small U , there is a one dimension center manifold for system (12) on which the dynamics of $E^*(u^*, v^*)$ is governed by

$$\frac{dU}{dt} = - \frac{l_1}{b_{10}(a_{10} + b_{01})} U^2 + O(|U|^3). \quad (13)$$

Since $l_1 \neq 0$, model (1) undergoes a saddle-node bifurcation at $E^*(u^*, v^*)$. \square

3.2. Hopf bifurcation. Model (1) undergoes a Hopf bifurcation at $E^*(u^*, v^*)$ if characteristic equation (8) has a pair of purely imaginary roots $\lambda = \pm i\omega$, i.e., when

$$\varphi(u^*) = a - \frac{q}{1+cu^*} \left(\frac{cpu^*}{m(1+cu^*)^2} - 1 \right) = 0. \quad (14)$$

Choosing the fear level k as the bifurcation parameter, we can determine the critical value $k = k_*$ from (14). In what follows, we determine the type of Hopf bifurcation at $k = k_*$. Similar to the analysis of saddle-node bifurcation, we shift $E^*(u^*, v^*)$ to the origin by the linear translation $\tilde{u} = u - u^*$ and $\tilde{v} = v - v^*$ and make the linear transformation

$$U_1 = -\frac{1}{a_{01}} \tilde{u}, \quad V_1 = \frac{1}{\omega} \left(\frac{a_{10}}{a_{01}} \tilde{u} + \tilde{v} \right), \quad (15)$$

then model (1) becomes

$$\begin{aligned} \frac{dU_1}{dt} &= -\omega V_1 + \sum_{2 \leq i+j \leq 3} A_{ij} U_1^i V_1^j + \mathcal{O}(|U_1, V_1|^4), \\ \frac{dV_1}{dt} &= \omega U_1 + \sum_{2 \leq i+j \leq 3} B_{ij} U_1^i V_1^j + \mathcal{O}(|U_1, V_1|^4), \end{aligned} \quad (16)$$

where

$$\begin{aligned}
A_{20} &= -a_{01}a_{20} + a_{10}a_{11} - \frac{a_{10}^2a_{02}}{a_{01}}, \quad A_{11} = a_{11}\omega - \frac{2a_{10}a_{02}\omega}{a_{01}}, \quad A_{02} = -\frac{a_{02}\omega^2}{a_{01}}, \\
A_{30} &= a_{01}^2a_{30} - a_{10}a_{01}a_{21} + a_{10}^2a_{12} - \frac{a_{10}^3a_{03}}{a_{01}}, \quad A_{03} = -\frac{a_{03}\omega^3}{a_{01}}, \\
A_{12} &= a_{12}\omega^2 - \frac{3a_{10}a_{03}\omega^2}{a_{01}}, \quad A_{21} = -a_{01}a_{21}\omega - \frac{3a_{10}^2a_{03}\omega}{a_{01}} + 2a_{10}a_{12}\omega, \\
B_{20} &= \frac{a_{10}a_{01}a_{20}}{\omega} + \frac{a_{01}^2b_{20}}{\omega} - \frac{a_{10}^2a_{11}}{\omega} - \frac{a_{10}a_{01}b_{11}}{\omega} + \frac{a_{10}^3a_{02}}{a_{01}\omega} + \frac{a_{10}^2b_{02}}{\omega}, \\
B_{11} &= -a_{10}a_{11} - a_{01}b_{11} + \frac{2a_{10}^2a_{02}}{a_{01}} + 2a_{10}b_{02}, \quad B_{02} = \frac{a_{10}a_{02}\omega}{a_{01}} + b_{02}\omega, \\
B_{30} &= -\frac{a_{10}a_{01}^2a_{30}}{\omega} - \frac{a_{01}^3b_{30}}{\omega} + \frac{a_{10}^2a_{01}a_{21}}{\omega} + \frac{a_{10}a_{01}^2b_{21}}{\omega} - \frac{a_{10}^3a_{12}}{\omega} + \frac{a_{10}^4a_{03}}{a_{01}\omega}, \\
B_{21} &= a_{10}a_{01}a_{21} + a_{01}^2b_{21} - 2a_{10}^2a_{12} + \frac{3a_{10}^3a_{03}}{a_{01}}, \\
B_{12} &= -a_{10}a_{12}\omega + \frac{3a_{10}^2a_{03}\omega}{a_{01}}, \quad B_{03} = \frac{a_{10}a_{03}\omega^2}{a_{01}}.
\end{aligned}$$

According to [17], the Lyapunov coefficient is

$$\begin{aligned}
\Lambda &= \frac{1}{16} (A_{30} + A_{12} + B_{21} + B_{03}) + \frac{1}{16\omega} (A_{11}(A_{20} + A_{02}) - B_{11}(B_{20} + B_{02}) \\
&\quad - A_{20}B_{20} + A_{02}B_{02}). \tag{17}
\end{aligned}$$

Therefore, we have the following result.

Theorem 3.2. *Suppose that $r > d$ and $E^*(u^*, v^*)$ is a positive equilibrium of model (1). If (14) and $h'(u^*) < 0$ hold, then when k passes across k^* , model (1) undergoes a subcritical (supercritical) Hopf bifurcation at $E^*(u^*, v^*)$ if $\Lambda > 0$ ($\Lambda < 0$).*

3.3. Bogdanov-Takens bifurcation. It is easy to know that characteristic equation (8) has two zero roots when u^* satisfies

$$\frac{krm^2}{(m + (mc + kq)u^*)^2} = \frac{m}{1 + cu^*} - \frac{p}{(1 + cu^*)^3}. \tag{18}$$

In this situation, model (1) has a nilpotent singularity. By making the following affine transformation:

$$U_2 = \tilde{u}, \quad V_2 = a_{10}\tilde{u} + a_{01}\tilde{v},$$

then system (11) becomes

$$\begin{aligned}
\frac{dU_2}{dt} &= V_2 + \hat{A}_{20}U_2^2 + \hat{A}_{11}U_2V_2 + \hat{A}_{02}V_2^2 + \mathcal{O}(|U_2, V_2|^3), \\
\frac{dV_2}{dt} &= \hat{B}_{20}U_2^2 + \hat{B}_{11}U_2V_2 + \hat{B}_{02}V_2^2 + \mathcal{O}(|U_2, V_2|^3),
\end{aligned} \tag{19}$$

where

$$\begin{aligned}
\hat{A}_{20} &= a_{20} - \frac{a_{11}a_{10}}{a_{01}} + \frac{a_{02}a_{10}^2}{a_{01}^2}, \quad \hat{A}_{11} = \frac{a_{11}}{a_{01}} - \frac{2a_{02}a_{10}}{a_{01}^2}, \quad A_{02} = \frac{a_{02}}{a_{01}^2}, \\
\hat{B}_{20} &= a_{01}b_{20} - a_{10}b_{11} + \frac{b_{02}a_{10}^2}{a_{01}} + a_{10}\hat{A}_{20}, \\
\hat{B}_{11} &= b_{11} - \frac{2a_{10}b_{02}}{a_{01}} + a_{10}\hat{A}_{11}, \quad \hat{B}_{02} = \frac{b_{02}}{a_{01}} + a_{10}\hat{A}_{02}.
\end{aligned} \tag{20}$$

By further performing a near-identity transformation as follows,

$$\begin{aligned} U_2 &= U_3 + \frac{1}{2}(\widehat{A}_{11} + \widehat{B}_{02})U_3^2 + \widehat{A}_{02}U_3V_3, \\ V_2 &= V_3 - \widehat{A}_{20}U_3^2 + \widehat{B}_{02}U_3V_3, \end{aligned} \quad (21)$$

we can obtain

$$\begin{aligned} \frac{dU_3}{dt} &= V_3 + \mathcal{O}(|U_3, V_3|^3), \\ \frac{dV_3}{dt} &= \overline{B}_{20}U_3^2 + \overline{B}_{11}U_3V_3 + \mathcal{O}(|U_3, V_3|^3), \end{aligned} \quad (22)$$

where $\overline{B}_{20} = \widehat{B}_{20}$ and $\overline{B}_{11} = \widehat{B}_{11} + 2\widehat{A}_{20}$. Now we introduce the transformation

$$\begin{aligned} U_4 &= U_3, \\ V_4 &= V_3 + \mathcal{O}(|U_3, V_3|^3), \end{aligned} \quad (23)$$

Then we obtain the the normal form

$$\begin{aligned} \frac{dU_4}{dt} &= V_4, \\ \frac{dV_4}{dt} &= \overline{B}_{20}U_4^2 + \overline{B}_{11}U_4V_4 + \mathcal{O}(|U_4, V_4|^3), \end{aligned} \quad (24)$$

It is difficult to determine the signs of \overline{B}_{20} and \overline{B}_{11} . We will solve this by computing $a_{01}^2\overline{B}_{20}$ and $a_{01}\overline{B}_{11}$. Here,

$$\begin{aligned} a_{01}^2\overline{B}_{20} &= a_{01}^3b_{20} - a_{01}^2a_{10}b_{11} + a_{01}b_{02}a_{10}^2 + a_{01}^2a_{10}a_{20} - a_{01}a_{10}^2a_{11} + a_{02}a_{10}^3 \\ &= \left(\frac{krm^2u^*(1+cu^*)^2}{(m+(mc+kq)u^*)^2} + \frac{pu^*}{1+cu^*} \right)^3 \frac{cq^2u^*}{m(1+cu^*)^4} - \left(\frac{krm^2u^*(1+cu^*)^2}{(m+(mc+kq)u^*)^2} \right. \\ &\quad \left. + \frac{pu^*}{1+cu^*} \right)^2 \left(-au^* + \frac{cpqu^{*2}}{m(1+cu^*)^3} \right) \frac{q}{(1+cu^*)^2} + m \left(\frac{pu^*}{1+cu^*} + \right. \\ &\quad \left. \frac{krm^2u^*(1+cu^*)^2}{(m+(mc+kq)u^*)^2} \right) \left(-au^* + \frac{cpqu^{*2}}{m(1+cu^*)^3} \right)^2 + \left(\frac{krm^2u^*(1+cu^*)^2}{(m+(mc+kq)u^*)^2} \right. \\ &\quad \left. + \frac{pu^*}{1+cu^*} \right)^2 \left(-au^* + \frac{cpqu^{*2}}{m(1+cu^*)^3} \right) \left(-a + \frac{cpqu^*}{m(1+cu^*)^4} \right) + \left(\frac{pu^*}{1+cu^*} \right. \\ &\quad \left. \frac{krm^2u^*(1+cu^*)^2}{(m+(mc+kq)u^*)^2} \right) \left(-au^* + \frac{cpqu^{*2}}{m(1+cu^*)^3} \right)^2 \left(\frac{-krm^2(1+cu^*)^2}{(m+(mc+kq)u^*)^2} \right. \\ &\quad \left. - \frac{p}{(1+cu^*)^2} \right) + \frac{k^2rm^3u^*(1+cu^*)^3}{(m+(mc+kq)u^*)^3} \left(-au^* + \frac{cpqu^{*2}}{m(1+cu^*)^3} \right)^3 \\ &= \frac{m^2cq^2u^{*4}}{1+cu^*} + \frac{mcpq^2u^{*4}(1-cu^*)}{(1+cu^*)^3} + \frac{k^2rm^3q^3u^{*4}}{(m+(mc+kq)u^*)^3} \\ &= \frac{1}{2}m^2qu^{*4}(1+cu^*) \left(\frac{2mrkq(cm+kq)}{(m+(mc+kq)u^*)^3} + \frac{2cpq(2-cu^*)}{m(1+cu^*)^4} \right) \\ &= \frac{1}{2}m^2qu^{*4}(1+cu^*)h''(u^*) \end{aligned} \quad (25)$$

and

$$a_{01}\overline{B}_{11} = \frac{-2mcqu^{*2}}{1+cu^*} + \frac{2cpqu^{*2}(2cu^*-1)}{(1+cu^*)^3} = -2mu^*(1+cu^*)\varphi'(u^*). \quad (26)$$

Since $a_{01} < 0$, $a_{01}^2\overline{B}_{20}$ has the same sign as \overline{B}_{20} , while $a_{01}\overline{B}_{11}$ has the opposite sign as \overline{B}_{11} . If $F_2(u^*) \neq 0$, then $h''(u^*) \neq 0$ for the positive equilibrium $E^*(u^*, v^*)$.

It then follows that $\overline{B}_{20} \neq 0$. Further when $\varphi'(u^*) \neq 0$, system (22) becomes the following normal form:

$$\begin{aligned} \frac{dU_5}{d\tau} &= V_5 \\ \frac{dV_5}{d\tau} &= \operatorname{sgn}(h''(u^*))U_5^2 + \operatorname{sgn}(\varphi'(u^*))U_5V_5 + \mathcal{O}(|U_5, V_5|^3), \end{aligned} \quad (27)$$

by making the following transformation

$$U_4 = \left| \frac{\overline{B}_{20}}{\overline{B}_{11}^2} \right| U_5, \quad V_4 = \left| \frac{\overline{B}_{20}^2}{\overline{B}_{11}^3} \right| V_5, \quad t = \left| \frac{\overline{B}_{11}}{\overline{B}_{20}} \right| \tau. \quad (28)$$

Therefore, according to Theorem 4.5 in [22], we know that $E^*(u^*, v^*)$ is a Bogdanov-Takens point of codimension 2.

As a summary, we have the following theorem.

Theorem 3.3. *Suppose that $r > d$ and $E^*(u^*, v^*)$ is a positive equilibrium of model (1). If (18) is satisfied, $\varphi'(u^*) \neq 0$, and $F_2(u^*) \neq 0$, then $E^*(u^*, v^*)$ is a Bogdanov-Takens point of codimension 2.*

Notice that if $F_2(u^*) = 0$, then model (1) may undergo bifurcations with codimension higher than 2. Here we do not discuss further for this case. In what follows, we consider the bifurcation of the degenerate equilibrium $E^*(u^*, v^*)$ when the parameters k and m vary in a small neighborhood of (k_{BT}, m_{BT}) , where (k_{BT}, m_{BT}) is determined by Theorem 3.3. To this end, we consider the following system

$$\begin{aligned} \frac{du}{dt} &= \frac{ru}{1 + (k_{BT} + \varepsilon_1)v} - du - au^2 - \frac{puv}{1 + cu}, \\ \frac{dv}{dt} &= -(m_{BT} + \varepsilon_2)v^2 + \frac{quv}{1 + cu}. \end{aligned} \quad (29)$$

Firstly, we transform $E^*(u^*, v^*)$ into the origin and thus obtain the following system

$$\begin{aligned} \frac{du}{dt} &= \tilde{a}_{00}(\varepsilon) + \sum_{1 \leq i+j \leq 2} \tilde{a}_{ij}(\varepsilon)u^i v^j + \mathcal{O}(|u, v|^3), \\ \frac{dv}{dt} &= \tilde{b}_{00}(\varepsilon) + \sum_{1 \leq i+j \leq 2} \tilde{b}_{ij}(\varepsilon)u^i v^j + \mathcal{O}(|u, v|^3). \end{aligned} \quad (30)$$

where $\varepsilon = (\varepsilon_1, \varepsilon_2)$ and

$$\begin{aligned} \tilde{a}_{00}(\varepsilon) &= \frac{ru^*}{1 + (k_{BT} + \varepsilon_1)v^*} - \frac{ru^*}{1 + kv^*}, \\ \tilde{a}_{10}(\varepsilon) &= \frac{r}{1 + (k_{BT} + \varepsilon_1)v^*} - d - 2a_{BT}u^* - \frac{pv^*}{(1 + cu^*)^2}, \\ \tilde{a}_{01}(\varepsilon) &= - \left(\frac{(k_{BT} + \varepsilon_1)ru^*}{(1 + (k_{BT} + \varepsilon_1)v^*)^2} + \frac{pu^*}{1 + cu^*} \right), \quad \tilde{a}_{20}(\varepsilon) = -a_{BT} + \frac{cpv^*}{(1 + cu^*)^3}, \\ \tilde{a}_{11}(\varepsilon) &= - \left(\frac{r(k_{BT} + \varepsilon_1)}{(1 + (k_{BT} + \varepsilon_1)v^*)^2} + \frac{p}{(1 + cu^*)^2} \right), \quad \tilde{a}_{02}(\varepsilon) = \frac{(k_{BT} + \varepsilon_1)^2 ru^*}{(1 + (k_{BT} + \varepsilon_1)v^*)^3}; \\ \tilde{b}_{00}(\varepsilon) &= -\varepsilon_2 v^{*2}, \quad \tilde{b}_{10}(\varepsilon) = \frac{qv^*}{(1 + cu^*)^2}, \quad \tilde{b}_{01}(\varepsilon) = -2(m_{BT} + \varepsilon_2)v^* + \frac{qu^*}{1 + cu^*}, \\ \tilde{b}_{20}(\varepsilon) &= -\frac{cqv^*}{(1 + cu^*)^3}, \quad \tilde{b}_{11}(\varepsilon) = \frac{q}{(1 + cu^*)^2}, \quad \tilde{b}_{02}(\varepsilon) = -(m_{BT} + \varepsilon_2). \end{aligned}$$

Making the following transformation

$$\begin{aligned} u_1 &= u, \\ v_1 &= \tilde{\alpha}_{00}(\varepsilon) + \sum_{1 \leq i+j \leq 2} \tilde{\alpha}_{ij}(\varepsilon) u^i v^j + \mathcal{O}(|u, v|^3), \end{aligned} \quad (31)$$

system (30) becomes

$$\begin{aligned} \frac{du_1}{dt} &= v_1, \\ \frac{dv_1}{dt} &= \tilde{\alpha}_{00}(\varepsilon) + \sum_{1 \leq i+j \leq 2} \tilde{\alpha}_{ij}(\varepsilon) u_1^i v_1^j + \mathcal{O}(|u_1, v_1|^3), \end{aligned} \quad (32)$$

where the coefficients $\tilde{\alpha}_{ij}$ ($0 \leq i+j \leq 2$) are provided in Appendix B.

Then by making the time scale transformation $dt = (1 - \tilde{\alpha}_{02}(\varepsilon)u_1)d\xi$, system (32) becomes

$$\begin{aligned} \frac{du_1}{d\xi} &= (1 - \tilde{\alpha}_{02}(\varepsilon)u_1)v_1, \\ \frac{dv_1}{d\xi} &= (1 - \tilde{\alpha}_{02}(\varepsilon)u_1) \left(\tilde{\alpha}_{00}(\varepsilon) + \sum_{1 \leq i+j \leq 2} \tilde{\alpha}_{ij}(\varepsilon) u_1^i v_1^j + \mathcal{O}(|u_1, v_1|^3) \right). \end{aligned} \quad (33)$$

Let $u_2 = u_1$, $v_2 = (1 - \tilde{\alpha}_{02}(\varepsilon)u_1)v_1$, we obtain that

$$\begin{aligned} \frac{du_2}{d\xi} &= v_2, \\ \frac{dv_2}{d\xi} &= \tilde{\beta}_{00}(\varepsilon) + \sum_{1 \leq i+j \leq 2} \tilde{\beta}_{ij}(\varepsilon) u_2^i v_2^j + \mathcal{O}(|u_2, v_2|^3), \end{aligned} \quad (34)$$

where

$$\begin{aligned} \tilde{\beta}_{00}(\varepsilon) &= \tilde{\alpha}_{00}(\varepsilon), & \tilde{\beta}_{10}(\varepsilon) &= \tilde{\alpha}_{10}(\varepsilon) - 2\tilde{\alpha}_{00}(\varepsilon)\tilde{\alpha}_{02}(\varepsilon), \\ \tilde{\beta}_{01}(\varepsilon) &= \tilde{\alpha}_{01}(\varepsilon), & \tilde{\beta}_{11}(\varepsilon) &= \tilde{\alpha}_{11}(\varepsilon) - \tilde{\alpha}_{01}(\varepsilon)\tilde{\alpha}_{02}(\varepsilon), \\ \tilde{\beta}_{20}(\varepsilon) &= \tilde{\alpha}_{20}(\varepsilon) - 2\tilde{\alpha}_{02}(\varepsilon)\tilde{\alpha}_{10}(\varepsilon) + \tilde{\alpha}_{02}^2(\varepsilon)\tilde{\alpha}_{00}(\varepsilon). \end{aligned}$$

We further assume that $u_3 = u_2 + \frac{\tilde{\beta}_{10}(\varepsilon)}{2\tilde{\beta}_{20}(\varepsilon)}$, $v_3 = v_2$, then

$$\begin{aligned} \frac{du_3}{d\xi} &= v_3, \\ \frac{dv_3}{d\xi} &= \tilde{\gamma}_{00}(\varepsilon) + \tilde{\gamma}_{10}(\varepsilon)u_3 + \tilde{\gamma}_{01}(\varepsilon)v_3 + \tilde{\gamma}_{20}(\varepsilon)u_3^2 + \tilde{\gamma}_{11}(\varepsilon)u_3v_3 + \mathcal{O}(|u_3, v_3|^3), \end{aligned} \quad (35)$$

where

$$\begin{aligned} \tilde{\gamma}_{00}(\varepsilon) &= \tilde{\beta}_{00}(\varepsilon) - \frac{\tilde{\beta}_{00}^2(\varepsilon)}{4\tilde{\beta}_{20}(\varepsilon)}, & \tilde{\gamma}_{01}(\varepsilon) &= \tilde{\beta}_{01}(\varepsilon) - \frac{\tilde{\beta}_{11}(\varepsilon)\tilde{\beta}_{10}(\varepsilon)}{2\tilde{\beta}_{20}(\varepsilon)}, \\ \tilde{\gamma}_{20}(\varepsilon) &= \tilde{\beta}_{20}(\varepsilon), & \tilde{\gamma}_{11}(\varepsilon) &= \tilde{\beta}_{11}(\varepsilon). \end{aligned}$$

Now let $u_4 = \frac{\tilde{\gamma}_{11}^2(\varepsilon)}{\tilde{\gamma}_{20}(\varepsilon)}u_3$, $v_4 = \frac{\tilde{\gamma}_{11}^3(\varepsilon)}{\tilde{\gamma}_{20}(\varepsilon)}v_3$ and $\xi' = \frac{\tilde{\gamma}_{20}(\varepsilon)}{\tilde{\gamma}_{11}(\varepsilon)}\xi$, we obtain

$$\begin{aligned} \frac{du_4}{d\xi'} &= v_4, \\ \frac{dv_4}{d\xi'} &= \tilde{\eta}_1(\varepsilon) + \tilde{\eta}_2(\varepsilon)v_4 + u_4^2 + u_4v_4 + \mathcal{O}(|u_4, v_4|^3), \end{aligned} \quad (36)$$

where

$$\tilde{\eta}_1(\varepsilon) = \frac{\tilde{\gamma}_{00}(\varepsilon)\tilde{\gamma}_{11}^4(\varepsilon)}{\tilde{\gamma}_{20}^3(\varepsilon)}, \quad \tilde{\eta}_2(\varepsilon) = \frac{\tilde{\gamma}_{01}(\varepsilon)\tilde{\gamma}_{11}(\varepsilon)}{\tilde{\gamma}_{20}(\varepsilon)}. \quad (37)$$

Therefore, according to the results in [17], we have the following bifurcation curves if the Jacobi matrix

$$\frac{\partial(\tilde{\eta}_1, \tilde{\eta}_2)}{\partial(\varepsilon_1, \varepsilon_2)} \neq 0, \quad (38)$$

- The saddle-node bifurcation curve: $SN = \{(\tilde{\eta}_1, \tilde{\eta}_2) | \tilde{\eta}_1 = 0, \tilde{\eta}_2 \neq 0\}$;
- The Hopf bifurcation curve: $H = \{(\tilde{\eta}_1, \tilde{\eta}_2) | \tilde{\eta}_2 = \sqrt{-\tilde{\eta}_1}, \tilde{\eta}_1 < 0\}$;
- The homoclinic-loop bifurcation curve: $HL = \{(\tilde{\eta}_1, \tilde{\eta}_2) | \eta_2 = \frac{5}{7}\sqrt{-\tilde{\eta}_1} + o(\tilde{\eta}_1), \tilde{\eta}_1 < 0\}$.

4. Bifurcation diagrams. Notice that when $r \leq d$, the trivial equilibrium $E^0(0, 0)$ is globally attractive, meaning that both the prey and predators will go to extinction eventually. This is an undesired situation. So, in this section, we always assume that $r > d$. It then follows from Theorem 2.3 that the half-trivial equilibrium $E^1(\frac{r-d}{a}, 0)$ is always an unstable saddle, and the stability of each positive equilibrium $E^*(u^*, v^*)$ is closely related to the bifurcations that model (1) undergoes.

Notice also that in the absence of the predators, $\frac{r-d}{a}$ is the environmental capacity of prey, which characters the amount of resources the environment could provide for the prey species. It is well known that environmental resources are fundamental to maintaining the sustainability of ecosystems. Generally, for a particular prey species, we can consider its natural birth rate (r) and death rate (d), and therefore its inherent growth rate ($r - d$) to be constant. Therefore, the density-dependent coefficient (a), which characters the intra-specific competition of prey species, should be a key factor affecting the dynamics of the model. Here we mainly focus our attention on how the fear effect in prey and crowding effect in predators affect the dynamics of model (1) under different levels of environmental resources (determined by different values of a). For this purpose, in this section, we always fix in model (1) the parameters

$$r = 1.8, d = 0.01, p = 0.7, c = 0.5, q = 0.66 \quad (39)$$

and vary k and m to numerically illustrate the dynamics that model (1) may have under different values of a .

To obtain a comprehensive understanding of the dynamics of model (1), we first observe the combined effect of predators' crowding and predator-induced fear on the dynamics of model (1) under different intensities of prey competition. The two-parameter bifurcation diagrams of model (1) drawn on the (k, m) -plane for different values of a are shown in Figure 1, from which we can see that the bifurcation diagrams can be very different for different values of a .

- When $a = 0.058$ (see Figure 1 (a)), only the saddle-node bifurcations occur in model (1). In this situation, there are two different cases:
 - ★ When (k, m) is seated in the green region, model (1) has three positive equilibria, the upper one and the lower one are stable and the middle one is an unstable saddle, see the region II in Figure 2 (a).
 - ★ When (k, m) is seated in the white region, model (1) has a unique positive equilibrium which is a global attractor, see the region I in Figure 2 (a) or Figure 3 (a) and (h).

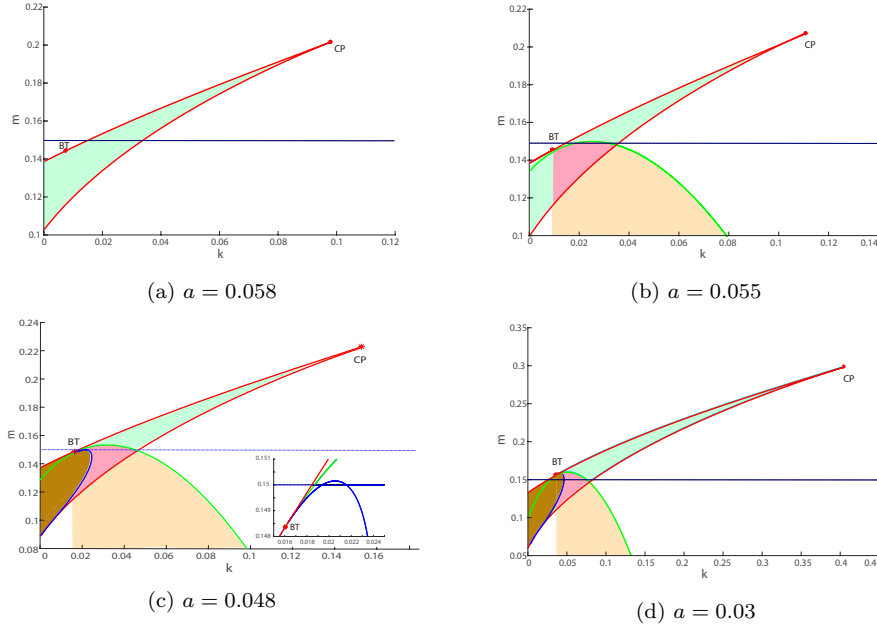


FIGURE 1. (Color online) Two-parameter bifurcation diagrams of system (1) on the (k, m) -plane for different competition intensities of prey: (a) $a = 0.058$, (b) $a = 0.055$, (c) $a = 0.048$ and (d) $a = 0.03$. The other parameters take the values as in (39). The label ‘BT’ denotes the Bogdanov-Takens bifurcation point and ‘CP’ the cusp point. The curves of saddle-node bifurcation (red), Hopf bifurcation (green) and homoclinic-loop bifurcation (blue) separate the (k, m) -plane into distinct regions. In the white regions, model (1) has a unique positive equilibrium which is globally stable, see the region I in Figure 2; In the green regions, model (1) has three positive equilibria: two stable and one unstable (saddle), see the region II in Figure 2; In the pink regions, model (1) has three equilibria and exhibits bistability between a positive equilibrium and a limit cycle (with an unstable positive equilibrium in it), see the region III in Figure 2; In the brown regions, model (1) has three positive equilibria and only the upper one is stable, see the region IV in Figure 2; In the yellow regions, model (1) has a unique positive equilibrium, which is surrounded by a stable limit cycle, see Figure 3 (g).

- When $a = 0.055$ (see Fig. 1 (b)), the (k, m) -plane is divided into four regions by the saddle-node bifurcation and Hopf bifurcation curves. Except for the two cases occurred in Figure 1 (a), model (1) can exhibit two other different dynamics:
 - ★ When (k, m) is seated in the pink region, model (1) possesses three positive equilibria and a stable limit cycle. In this case, model (1) shows bistability between a stable positive equilibrium and a stable limit cycle, see the region III in Figure 2 (b).

- ★ When (k, m) is seated in the yellow region, model (1) has a positive equilibrium which is surrounded by a stable limit cycle. In this case, the limit cycle is the unique attractor for model (1), see Figure 3 (g).
- When $a = 0.048$ (see Figure 1 (c)), the (k, m) -plane is divided into five parts by the saddle-node bifurcation, Hopf bifurcation, and homoclinic-loop bifurcation curves. In this case, a kind of new dynamics emerges due to homoclinic-loop bifurcation: model (1) has three positive equilibria, but only one of them is stable, see the region IV in Figure 2 (c) or Figure 3 (c).
- When $a = 0.03$ (see Figure 1 (d)), no other new bifurcations occur compared to that when $a = 0.048$. However, even if we take the same values for k and m in Figures 1 (c) and (d), model (1) may show distinct dynamics. This observation indicates that it is necessary to show the bifurcation diagram for the convenience of further discussion though they seem similar.

These results indicate that both fear effect in prey and crowding effect in predators play a significant role in the dynamics of model (1). For a more specific understanding of the respective effects of these two factors, one can fix one parameter and vary another one. Here, let us discuss the impact of fear effect as an example by fixing $m = 0.15$. The related results are shown in Figure 2:

- For strong prey competition (see Figure 2 (a), where $a = 0.058$), model (1) undergoes two saddle-node bifurcations at $k = 0.015051$ and $k = 0.033728$, between which a bistable region is established. As shown the region II in Figure 2 (a), model (1) shows a kind of bistability between two stable positive equilibria.
- As the prey competition intensity declines, say $a = 0.055$, we can see from Figure 2 (b) that model (1) undergoes two saddle-node bifurcations at $k = 0.016001$ and $k = 0.036801$. In addition, at $k = K_H^{(1)} = 0.019201$ and $k = K_H^{(2)} = 0.030579$, the lyapunov coefficients are $\Lambda = -0.0011391$ and $\Lambda = -0.00052573$, respectively, and therefore two supercritical Hopf bifurcations occur respectively at $k = K_H^{(1)}$ and $k = K_H^{(2)}$ on the lower branch of bifurcation diagram, and model (1) exists a stable limit cycle when $K_H^{(1)} < k < K_H^{(2)}$. Therefore there may exist two types of bistability: either between two stable positive equilibria (i.e., the region II in Figure 2 (b)) or between a stable positive equilibrium and a stable limit cycle (i.e., the region III in Figure 2 (b)).
- As a is further reduced to $a = 0.048$, we can see from Figure 2 (c) that model (1) undergoes two saddle-node bifurcations respectively at $k = k_{SN}^{(1)} = 0.018447$ and $k = k_{SN}^{(2)} = 0.046184$. In addition, model (1) undergoes two supercritical Hopf bifurcations respectively at $k = K_H^{(1)} = 0.018694$ and $k = K_H^{(2)} = 0.044595$ on the lower branch of bifurcation diagram (the Lyapunov coefficients are $\Lambda = -0.0034041$ and $\Lambda = -0.0003092667$, respectively). Specifically,
 - (a) when $k_{SN}^{(1)} < k < K_H^{(1)}$, the corresponding smallest positive equilibrium is linearly stable; when $k > K_H^{(1)}$, it becomes unstable and a bifurcating stable limit cycle emerges, which will disappears at the Homoclinic loop at $k = 0.019362$.

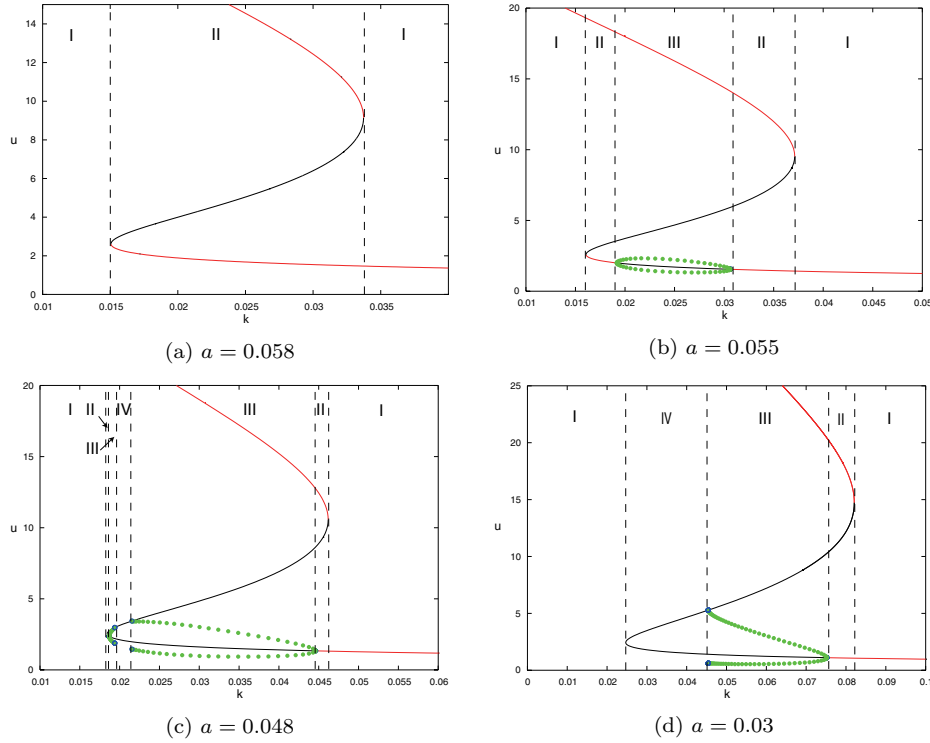


FIGURE 2. (Color online) Bifurcation diagram of model (1) with respect to the fear level k . The other parameters except a are taken as $r = 1.8$, $d = 0.01$, $p = 0.7$, $c = 0.5$, $m = 0.15$, $q = 0.66$. The red/black curves denote the stable/unstable equilibria respectively. The green dotted curves denote the stable limit cycles. The black dashed lines are located at bifurcation points to separate the distinct regions: (I) model (1) has a unique positive equilibrium, which is stable; (II) model (1) shows a type of bistability between which two stable positive equilibria; (III) model (1) shows a type of bistability between which a stable positive equilibrium and a stable interior limit cycle; (IV) model (1) has three positive equilibria and the upper one is stable.

- (b) when $k > K_H^{(2)}$, the corresponding smallest positive equilibrium is linearly stable, when $k < K_H^{(2)}$, it becomes unstable and a bifurcating stable limit cycle emerges, which will disappears at a Homoclinic loop at $k = 0.021601$.

In this scenario, model (1) can exhibit two types of bistability: between two stable positive equilibria (i.e., the region II in Figure 2 (c)) or between a stable positive equilibrium and a stable limit cycle (i.e., the region III in Figure 2 (c)). Each bistability phenomenon occurs for different intervals of the fear level k .

- Finally, for weak prey competition, say $a = 0.03$, we can see from Figure 2 (d) that model (1) undergoes two saddle-node bifurcations at $k = k_{SN}^{(1)} = 0.025001$ and $k = k_{SN}^{(2)} = 0.081998$ and a supercritical Hopf bifurcations at $k = k_H =$

0.075105 on the lower branch of bifurcation diagram (the Lyapunov coefficient is $\Lambda = 0.000060194$). When $k > k_H$, the corresponding smallest positive equilibrium is stable; When $k < k_H$, it loses its stability and a stable limit cycle emerges, which disappears at the Homoclinic loop at $k = 0.04540736$. In this situation, model (1) also has similar types of bistability as the above two situations (see the regions II and III in Figure 2 (d)).

For the influence of the predators' crowding effect, one can observe a similar phenomenon to Figure 2 and we will not repeat it here. In particular, we shall point out that how the predators' crowding effect affect the model dynamics for different intensities of prey competition if the indirect effects of predation are ignored (see the vertical axis in Figure 1). For strong prey competition, we can see from Figures 1 (a) and (b) that there exists two critical values m_1, m_2 (assume $m_1 < m_2$) of the predators' crowding effect parameter such that model (1) shows a bistability between two stable positive equilibria if $m_1 < m < m_2$ and monostable phenomenon if $m < m_1$ or $m > m_2$. For weak prey competition (see Figure 1 (c)), model (1) only shows the monostable phenomenon. These results imply that weak prey competition is easier to maintain the robustness of the model in the absence of fear effect.

Finally, we present an example to illustrate the impact of the fear level on the dynamics of model (1) for fixed a and m from the view of phase plane analysis.

An example. By taking $a = 0.048$ and $m = 0.137$, we can observe from Figure 3 that model can show distinct dynamics for different fear levels.

- (1) When the fear is very weak (see Figure 3 (a) where $k = 0.004$), model (1) has a unique positive equilibrium E^* , which is a global attractor.
- (2) As k is increased to $k = 0.004696115100001$ (see Figure 3 (b)), a positive equilibrium $E_{1,2}^*$ of multiplicity 2 emerges and thus model (1) has two positive equilibria $E_{1,2}^*$ and E_3^* .
- (3) As k increases, say $k = 0.04$ (see Figure 3 (c)), $E_{1,2}^*$ splits into two positive equilibria E_1^* and E_2^* , and then model (1) has three positive equilibria E_1^* , E_2^* and E_3^* , between which only the upper one E_3^* is stable.
- (4) If we further increase k to $k = 0.04293$ (see Figure 3 (d)), model (1) has three positive equilibria E_1^* , E_2^* and E_3^* (where $u_1^* < u_2^* < u_3^*$), between which E_3^* is stable, the middle saddle point E_2^* is connected by a homoclinic loop, which encloses the lower equilibrium E_1^* .
- (5) As k continues to increase, say $k = 0.058$ (see Figure 3 (e)), model (1) still has three positive equilibria E_1^* , E_2^* and E_3^* , and a stable limit cycle enclosing E_1^* .
- (6) In particular, when $k = 0.06503401$ (see Figure 3 (f)), E_2^* and E_3^* coincide into a positive equilibrium $E_{2,3}^*$ of multiplicity 2. In this case, model (1) has two positive equilibria E_1^* , $E_{2,3}^*$, and a stable limit cycle enclosing E_1^* .
- (7) If k is further increased, say $k = 0.075$ (see Figure 3 (g)), $E_{2,3}^*$ disappears and thus model (1) only has a unique positive equilibrium E_1^* denoted as E^* , which is unstable and enclosed by a stable limit cycle. In this situation, the limit cycle is the unique attractor.
- (8) Finally, as k increases such that the point $(k, 0.137)$ across the Hopf bifurcation curve, model (1) has only one positive equilibrium E^* , which is also the unique attractor (see Figure 3 (h)).

The above discussions indicate that model (1) shows complex dynamics and even two types of bistability either between two stable positive equilibria or between a

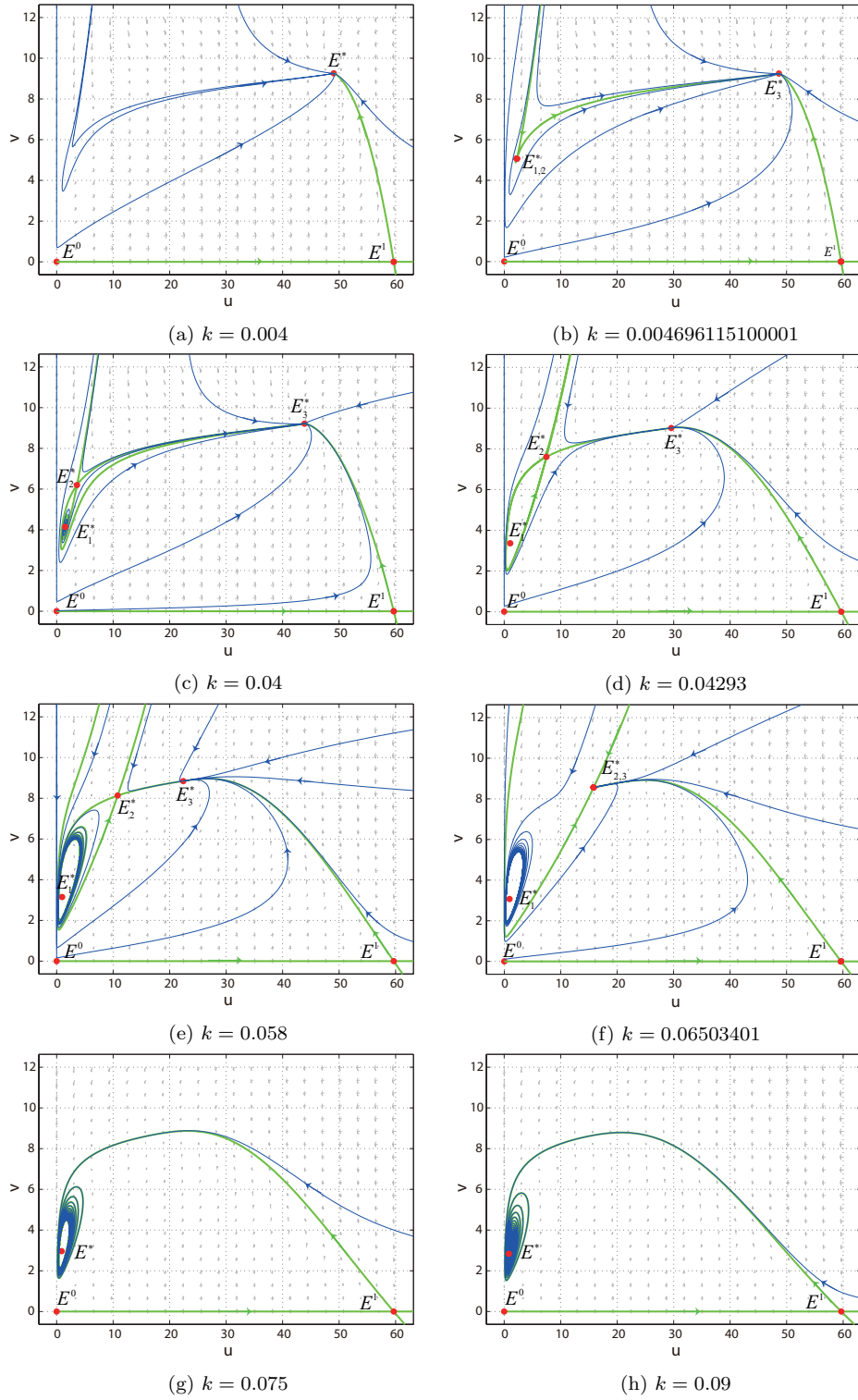


FIGURE 3. (Color online) Phase plane diagrams of model (1) with $m = 0.137$. The other parameters except k are the same as that in Figure 1 (c).

stable positive equilibrium and a stable limit cycle. These phenomena mean that the model has weak robustness and is highly vulnerable to environmental fluctuations.

5. Noise-induced transitions. To see how the environmental perturbations will affect the dynamics of model (1), it is necessary to discuss in the framework of stochastic differential equation model. Following the method in [10], we include the randomness into model (1), which yields the following stochastic model:

$$\begin{aligned} du &= \left(\frac{ru}{1+kv} - du - au^2 - \frac{puv}{1+cu} \right) dt + \sigma_1 u dB_1, \\ dv &= \left(-mv^2 + \frac{quv}{1+cu} \right) dt + \sigma_2 v dB_2, \end{aligned} \quad (40)$$

where $B_i(t)$ ($i = 1, 2$) are two standard one-dimensional independent Brownian motions and σ_i ($i = 1, 2$) are the noise intensities. For stochastic model (40), the existence and uniqueness of global positive solution can be directly obtained from Theorem 2.1 in [29].

In this section, we aim to study how environmental noises affect the dynamics of stochastic model (40), especially for the phenomena of noise-induced transitions between two different attractors in the scenarios when deterministic model (1) possesses bistability. For the convenience of discussion, we assume that $\sigma_1 = \sigma_2 = \sigma$.

5.1. Bistability between two positive equilibria. We first consider the scenario when determined model (1) possesses the bistability between two stable positive equilibria. For this purpose, we take in model (1) $m = 0.15$, $a = 0.058$, $k = 0.0337$, and other parameters take the same values as listed in (39). Then model (1) has a trivial equilibrium $E^0(0, 0)$, a semi-trivial equilibrium $E^1(30.8621, 0)$, and three coexistence equilibria $E_1^*(1.4692, 3.7268)$, $E_2^*(8.8890, 7.1837)$ and $E_3^*(9.4121, 7.2578)$. It is easy to check that E^0 is unstable, E^1 and E_2^* are two saddles, and both E_1^* and E_3^* are locally asymptotically stable. The corresponding phase plane diagram is shown in Figure 4, where the red-dotted curve (separatrix)¹ stands for the two stable manifolds of E_2^* which separates the first positive quadrant into two parts: the attraction basins of E_1^* and E_3^* . If the initial value is within the separatrix, then the solution of model (1) will converge to E_1^* , otherwise it converges to E_3^* .

When environmental noise is considered, the solution trajectory will change. In general, as the noise intensity increases, the solution starting from an initial point near a stable equilibrium, say E_1^* (or E_2^*), it will leave E_1^* (or E_2^*) and expand outward gradually. Once the stochastic trajectory crosses the separatrix and enters the attraction basin of E_2^* (or E_1^*), we can observe the noise induced transitions between the two attractors. To estimate the critical noise intensity values for the occurrence of noise induced transitions, we construct some confidence ellipses by the techniques of stochastic sensitivity functions. One can refer to [1, 2, 30, 31] for more details in this direction. Some necessary steps to obtain the confidence ellipse equation are shown in Appendix C. For the same parameters as in Figure 4, we can obtain the confidence ellipse equation of E_1^*

$$\begin{aligned} &0.001082(u - 1.4692)^2 - 0.001473(u - 1.4692)(v - 3.7268) \\ &+ 0.0008848(v - 3.7268)^2 = -2\sigma^2 \ln(1 - P), \end{aligned} \quad (41)$$

¹The separatrix are approximately obtained by using the interactive tool pplane 8 on Matlab for studying planar autonomous systems.

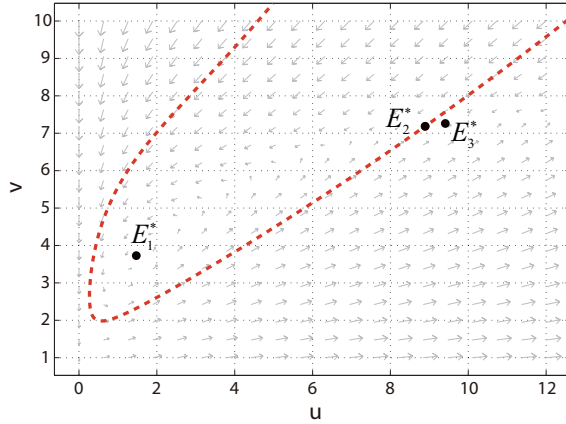


FIGURE 4. (Color online) Phase plane diagram of model (1) with $d = 0.01$, $p = 0.7$, $k = 0.0337$, $c = 0.5$, $q = 0.66$, $r = 1.8$, $a = 0.058$, $m = 0.15$. The red-dotted curve stands for the separatrix of two attraction basins.

and that of E_3^*

$$\begin{aligned} &0.0006906(u - 9.4121)^2 - 0.008455(u - 9.4121)(v - 7.2578) \\ &+ 0.03302(v - 7.2578)^2 = -2\sigma^2 \ln(1 - P). \end{aligned} \quad (42)$$

In Figure 5, we take $P = 0.95$, which means that if the initial point is near E_1^* , then the stochastic state of stochastic model (40) is distributed inside the ellipse with probability P (see Figure 5 (a)). In addition, we show the confidence ellipses of E_1^* with $\sigma = 0.007$, 0.0106 , 0.0125 in Figure 5 (b), from which we can see that the ellipse expands outward as σ increases. When $\sigma = \sigma_1 = 0.0106$, the ellipse is tangent to the separatrix of two attraction basins. σ_1 is called the critical noise intensity for the noise-induced transition's onset. If $\sigma > \sigma_1$ (see the large ellipse in Figure 5 (b)), the ellipse crosses the separatrix, the noise induced transition from E_1^* to E_3^* occurs. By the same way we can find another critical noise value $\sigma = \sigma_2 = 0.0041$ for the occurrence of transition from E_3^* to E_1^* . Obviously, $\sigma_1 > \sigma_2$.

We now consider two confidence ellipses together to explore the transition phenomenon induced by environmental fluctuations (see Figure 6):

- If the noise is weak, e.g., $\sigma = 0.004 < \sigma_2$, two confidence ellipses of E_1^* and E_3^* are strictly separated by the separatrix of two attraction basins (see the first picture of Figure 6 (a)). The solutions of stochastic model (40) with the initial values near E_1^* and E_3^* fluctuate respectively around them (see the second and third pictures of Figure 6 (a)). In this case, the stochastic probability density (SPD) of populations has a single peak (see the fourth pictures of Figure 6 (a)).
- As the noise intensity increases, the confidence ellipses expand outward gradually. When $\sigma_2 < \sigma < \sigma_1$, say $\sigma = 0.01$, the confidence ellipse of E_3^* crosses the separatrix into the attraction basin of E_1^* (see the first picture of Figure 6 (b)), then the solution starting from the vicinity of E_3^* may eventually switch to fluctuate around E_1^* with a high probability (the second picture of Figure 6 (b)). The corresponding stochastic trajectories and SPD are shown in the

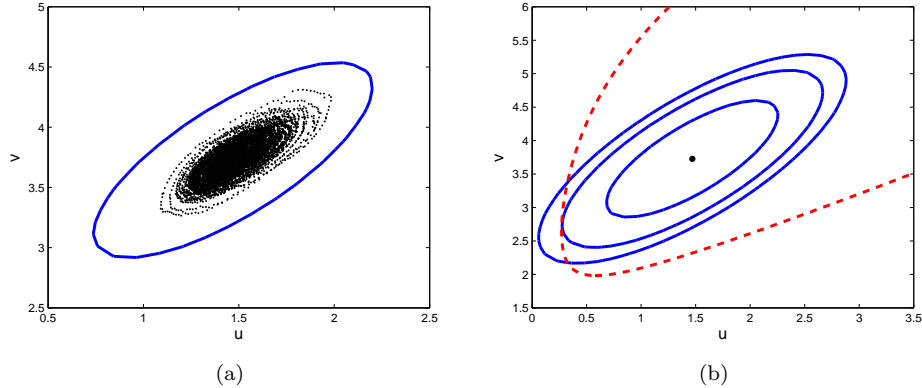


FIGURE 5. (Color online) (a) Random state (black-dotted) of stochastic model and confidence ellipse (blue-solid) of E_1^* for $\sigma = 0.0065$ and $P = 0.95$. (b) Separatrix of two attraction basins (red-dotted), and confidence ellipses (blue-solid) for $\sigma = 0.007$ (small), $\sigma = 0.0106$ (middle), $\sigma = 0.0125$ (large). The parameters are taken as $d = 0.01$, $p = 0.7$, $k = 0.0337$, $c = 0.5$, $q = 0.66$, $r = 1.8$, $a = 0.058$, $m = 0.15$.

third and fourth pictures of Figure 6 (b), where the SPD has two peaks. If σ continues to increase such that $\sigma > \sigma_1$, a symmetric case will occur, where the solutions starting from the vicinity of E_1^* eventually switch to fluctuate near the equilibrium E_3^* with a high probability. Here we do not display the related figures.

- If the noise intensity is large enough, say $\sigma = 0.05$, such that the two confidence ellipses of E_1^* and E_3^* coincide partially (see the first picture of Figure 6 (c)), and in this case noise induced frequent transitions appear. One can see the second picture of Figure 6 (c) for the corresponding time series diagram, the third picture of Figure 6 (c) for the stochastic trajectory diagram, and the fourth picture of Figure 6 (c) for the SPD.

5.2. Between a positive equilibrium and a limit cycle. We then consider the scenario when determined model (1) possesses the bistability between a positive equilibrium and a stable limit cycle. To this end, we take $m = 0.137$, $a = 0.03$, $k = 0.065$, and other parameters take the same values as listed in (39). The information of equilibria of model (1) is as follows: $E^0(0, 0)$ and $E_1^*(0.9330, 3.0649)$ are unstable, $E_2^*(15.4354, 8.5298)$ is a saddle, $E_3^*(16.2191, 8.5774)$ is locally asymptotically stable, and there exists a stable limit cycle enclosing E_1^* . The corresponding phase plane diagram is shown in Figure 7, where the red-dotted curve (separatrix) stands for the stable manifold of E_2^* which separates the first positive quadrant into two parts: the attraction basins of E_1^* and limit cycle (denoted by the purple curve). If the initial value is within the separatrix, then the solution of model (1) will converge to the limit cycle, otherwise it converges to E_3^* .

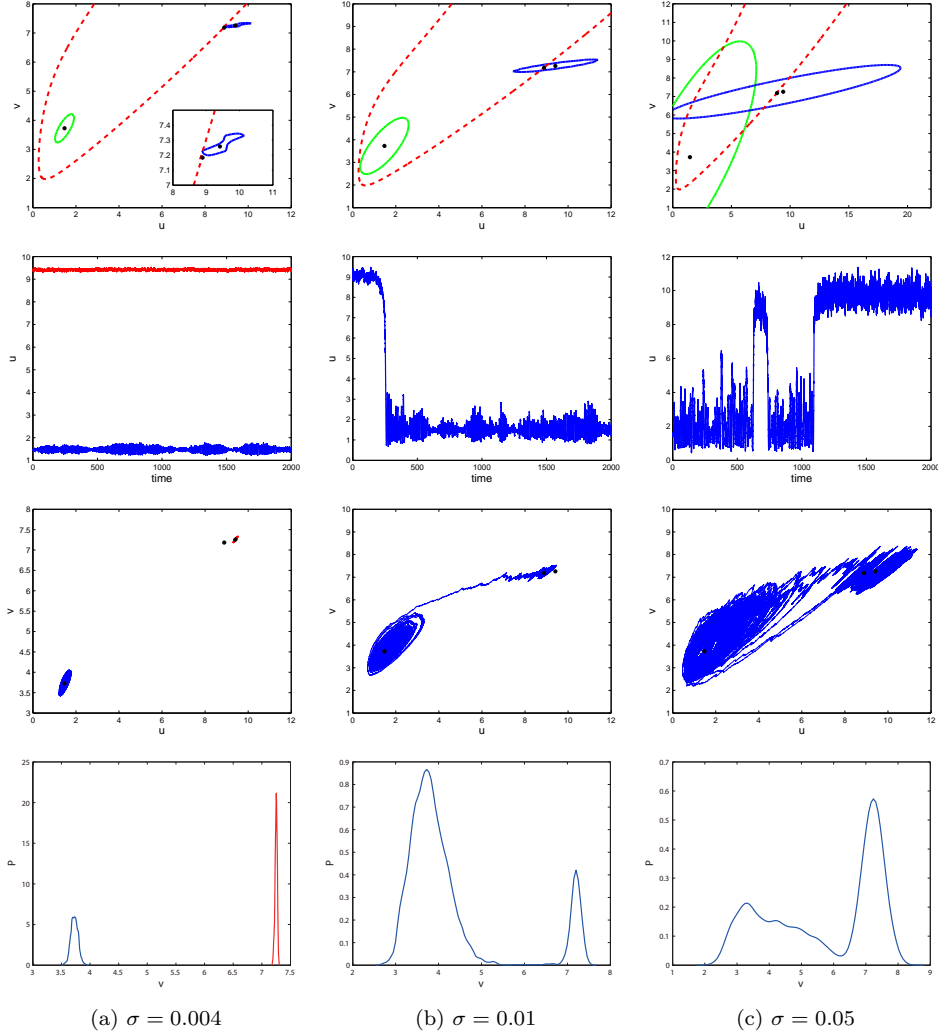


FIGURE 6. (Color online) Confidence domains, time series diagrams, phase plane diagrams, and stochastic probability density of stochastic model (40) for different noise intensity. The parameters are taken as $d = 0.01$, $p = 0.7$, $k = 0.0337$, $c = 0.5$, $q = 0.66$, $r = 1.8$, $a = 0.058$, $m = 0.15$.

For the equilibrium E_3^* , we can obtain its confidence ellipse equation by using the method in Appendix C,

$$0.0001488(u - 16.2191)^2 - 0.003079(u - 16.2191)(v - 8.5774) + 0.02868917462(v - 8.5774)^2 = -2\sigma^2 \ln(1 - P). \quad (43)$$

By using (43), analyzing as above we can estimate the critical noise intensity is $\sigma = \sigma_1 = 0.0031$, at which the confidence ellipse is tangent to the separatrix of two attraction basins.

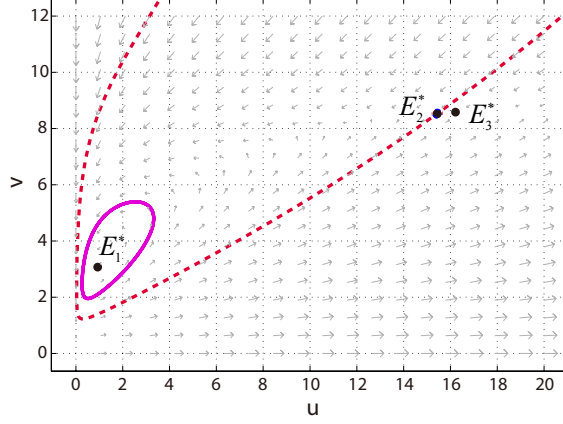


FIGURE 7. (Color online) Phase plane diagram of model (1) with $d = 0.01$, $p = 0.7$, $k = 0.065$, $c = 0.5$, $q = 0.66$, $r = 1.8$, $a = 0.03$, $m = 0.137$. The red-dotted curve stands for the separatrix of two attraction basins; the purple curve stands for the stable limit cycle.

For the limit cycle, for convenience, we denote it as $\mathcal{T}(u(t), v(t))$, $t \in [0, T]$, where T is the period. By using (44) in Appendix C, the boundaries of confidence bands of limit cycle \mathcal{T} can be determined. We show the confidence bands for $P = 0.95$ in Figure 8, where the pink curve stands for the limit cycle of the determined model (1), the green and blue curves stand for the boundaries of its confidence bands. It is easy to see that the confidence bands are seated on different sides of the limit cycle. In addition, the stochastic states are concentrated in the region enclosed by the confidence bands with a high probability (see Figure 8 (a)). As the noise intensity σ increases, the boundaries of the confidence bands also expand outward (see Figure 8 (b)). Therefore, we conclude that there exists a critical noise intensity such that the corresponding boundary is tangent to the separatrix of two attraction basins. Here the critical noise intensity is estimated as $\sigma = \sigma_2 = 0.061$. If the noise intensity is larger than σ_2 , then the stochastic states of model (40) is much likely to enter the attraction basin of E_3^* , and thus the solution eventually converges to E_3^* .

We now consider the confidence band of limit cycle \mathcal{T} and confidence ellipse of equilibrium E_3^* together to show some interesting transition phenomenon induced by environmental fluctuations. Four distinct phenomena can be observed for different noise intensities:

- For weak noise, say $\sigma = 0.003 < \sigma_1$, the confidence band of \mathcal{T} and the confidence ellipse of E_3^* are located on both sides of the boundary between the two attractive domains, respectively (see Figure 9 (a)). The solutions of stochastic model (40) with the initial values near E_3^* and \mathcal{T} of model (1) fluctuate respectively around them (see the left or middle panel of Figure 10 (a)). In this case, the SPD of populations has a single peak (see the right panel of Figure 10 (a)).
- As the noise intensity increases, the confidence band and confidence ellipse expands outward gradually, then the confidence region of E_3^* may cross the separatrix into the attraction basin of the limit cycle \mathcal{T} (see Figure 9 (b) where $\sigma_1 < \sigma = 0.05 < \sigma_2$), and the solutions starting from the vicinity of E_3^* may

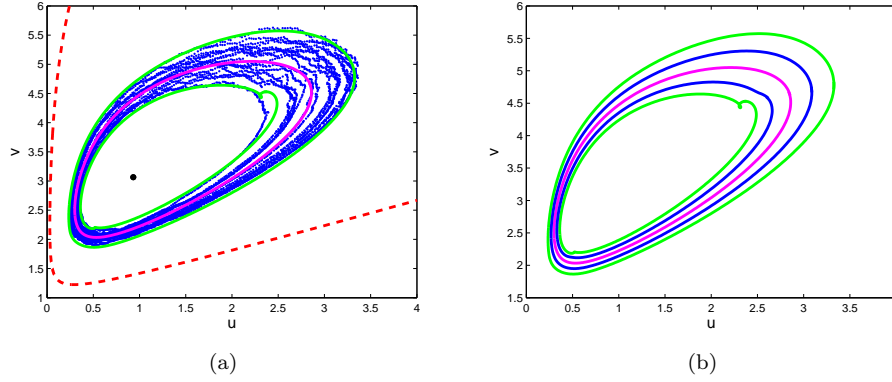


FIGURE 8. (Color online) Stochastic states and confidence bands of limit cycle for stochastic model (40) with $d = 0.01$, $p = 0.7$, $k = 0.065$, $c = 0.5$, $q = 0.66$, $r = 1.8$, $a = 0.03$, $m = 0.137$. (a) Separatrix of two attraction basins (red-dotted), stochastic states (blue) around determined cycle (pink), and confidence bands (green) for $\sigma = 0.02$. (b) Confidence bands for different noise intensity $\sigma = 0.01$ (blue) and $\sigma = 0.02$ (green).

eventually switch to fluctuate along \mathcal{T} with a high probability (the left panel of Figure 10 (b)). In this case, the SPD of populations has two peaks. The corresponding stochastic trajectories and SPD are shown in the middle and right panels of Figure 10 (b).

- If the noise intensity continues to increase, say $\sigma = 0.07 > \sigma_2$, the confidence band of \mathcal{T} may cross the separatrix into the attraction basin of E_3^* (see Figure 9 (c)), and the solutions starting from the vicinity of \mathcal{T} may eventually switch to fluctuate near the equilibrium E_3^* with a high probability (the left panel of Figure 10 (c)). The corresponding stochastic trajectories and SPD in this situation are shown in the middle and right panel of Figure 10 (c).
- Finally, if the noise intensity is large enough, for example $\sigma = 0.09$, we can see that the confidence band of \mathcal{T} and the confidence ellipse of E_3^* are intersected (see Figure 9 (d)), and in this case frequent transitions may appear. One can see the left panel of Figure 10 (d) for the corresponding time series, the middle panel of Figure 10 (d) for stochastic trajectory diagrams, and the right panel of Figure 10 (d) for the SPD.

6. Discussion. The interaction between predator and prey is a complex process in ecosystems, which can be influenced by many external environmental factors such as climatic variations, and internal factors such as births, deaths, aggregation behavior and habitat complexity. Assuming that prey and predator populations are at two different adjacent trophic levels in the same food chain of an ecosystem, in this paper, we consider a predator-prey model with fear effect in prey and crowding effect or self-limitation in predators.

For the scenario without considering external environmental perturbations, we first investigate the dynamics of the determined model (1). Our bifurcation results show that model (1) has at least one and at most three positive equilibria, and the number of positive equilibria is determined by the saddle-node bifurcation curves.

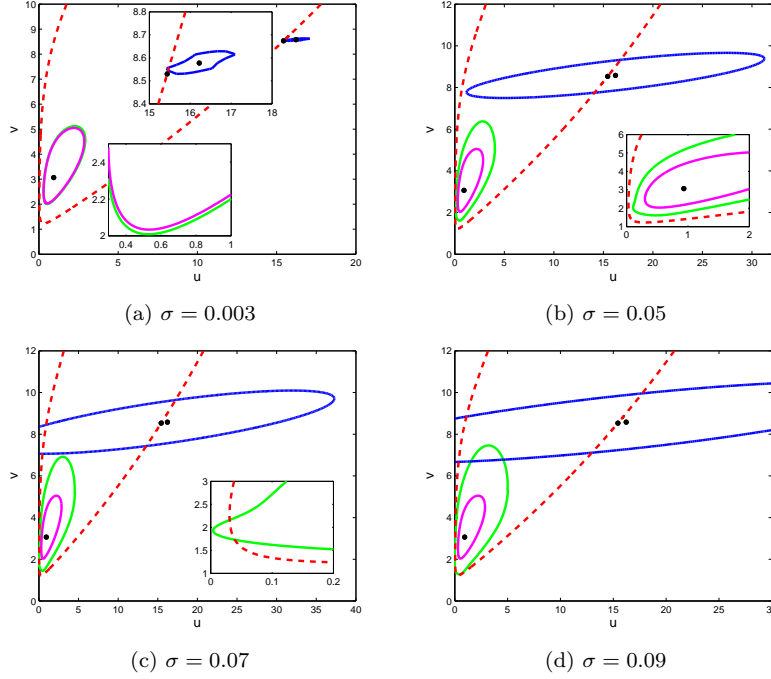


FIGURE 9. (Color online) Confidence domains of stochastic model for different noise intensities. The parameters are taken as $d = 0.01$, $p = 0.7$, $k = 0.065$, $c = 0.5$, $q = 0.66$, $r = 1.8$, $a = 0.03$, $m = 0.137$.

In the regions enclosed by the saddle-node bifurcation curves, model (1) has three positive equilibria, while outside this region, model (1) has a unique positive equilibrium. Under the situation where other bifurcations cannot occur, this region is a bistable region, in which two stable positive equilibria coexist (see the green region in Figure 1 (a)). If Hopf bifurcation further occurs, a stable (unstable) limit cycle will emerge. In this case, the stability of the positive equilibrium will change. In a range of the suitable parameters, there exists a bistability that a stable positive equilibrium and a stable limit cycle coexist (see the pink region in Figure 1 (b)). Moreover, as shown in Theorem 3.3, a Bogdanov-Takens bifurcation may occur and thus a homoclinic loop bifurcation curve may emerge. In this situation, a homoclinic loop will emerge (see Figure 3 (d) for the representative phase plane diagram). As the parameter further changes, the homoclinic loop will break and the related equilibrium will not regain its stability. Therefore, there is a situation will occur where model (1) has three positive equilibria, but only one of them is stable (see the brown region in Figures 1 (c) and (d)). These complex bifurcations and bistability phenomena suggest that the model dynamics is easily affected by external environmental fluctuations. We then study the developed stochastic model (40) and particular attention is devoted to the noise-induced transitions when model (1) shows bistability. By using the method of stochastic sensitive analysis, we numerically estimate the tipping points for the occurrence of transitions.

Among these above results, we observe two kinds of possible critical mechanisms: bifurcation-induced and noise-induced tipping. One bifurcation-induced tipping can

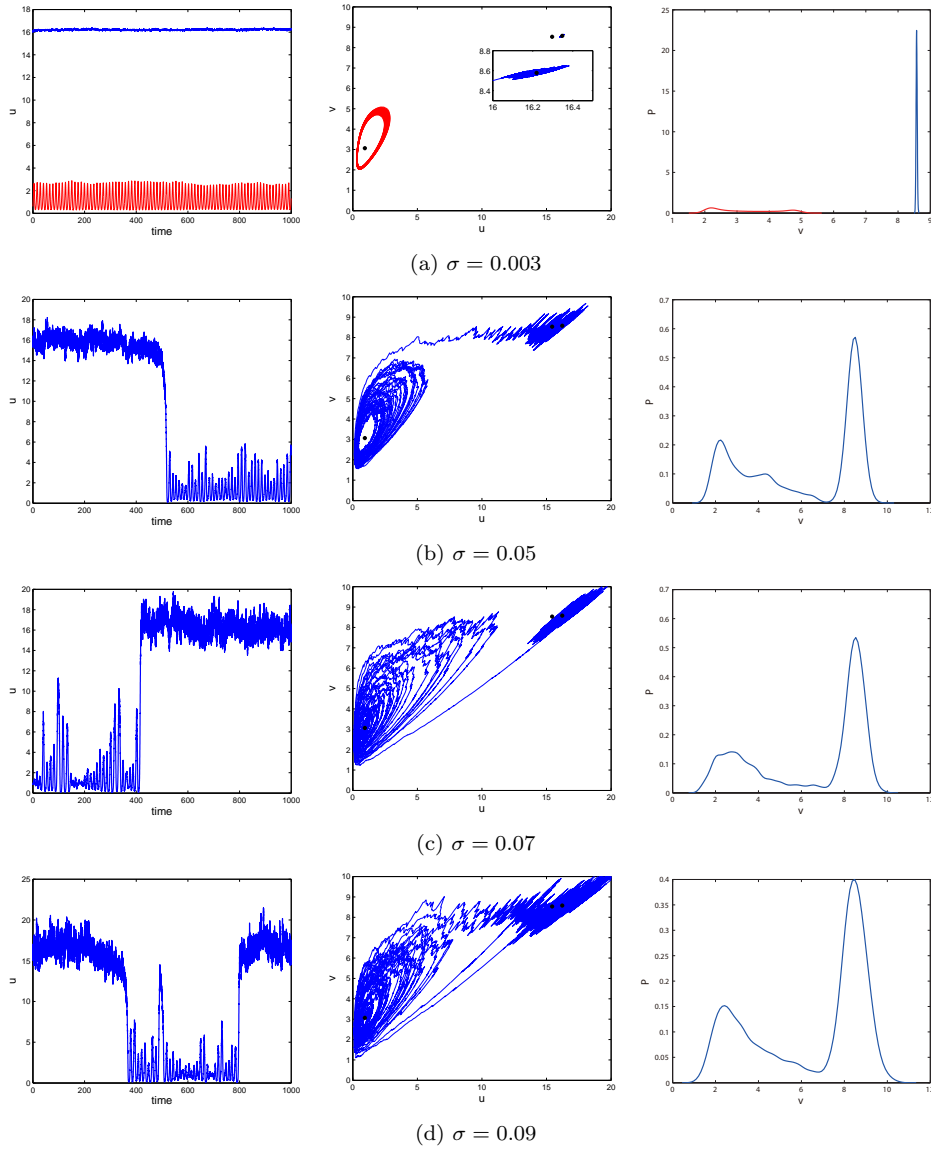


FIGURE 10. (Color online) Time series diagrams, phase plane diagrams, and stochastic probability density of stochastic model (40) for different noise intensities. The other parameters are the same as that in Figure 9.

be observed in Figure 2, where we show the relationship between the prey density and the fear level. The tipping values of fear level can be determined by saddle-node bifurcation points. It can be seen if the fear is smaller than the lower tipping value, the prey population is distributed in a relatively ideal state (i.e., high density); while if the fear is larger than the upper tipping value, the prey population may undergo a abrupt decrease and then is distributed in a relatively 'undesired' state (i.e., low density). The noise-induced tipping mechanism can be observed in Figures

6 and 10 from which we can see that a large noise intensity can induce the prey to switch from a high-level density to a low-level density fluctuation with a high probability, or even frequently switch between these two different modes. Therefore, the occurrence of some tipping points may drive the population into a less than ideal state, thus posing great difficulties in protecting ecosystem stability.

Intermediate predators are in the middle of the food chain, therefore they are inevitably affected by the fear from top predators. To understand the cascading effect of fear in food chains, some researchers considered the food chain systems in which the intermediate predators are assumed to be conformed to the linear death rate [9, 15]. They found that all types of fear can respectively stabilize the system by period-halving bifurcation. However, if there exist two types of fears, some complex phenomena emerge. For example, if the fears of intermediate predators and basal prey are considered simultaneously, the populations have periodic oscillations when these two fears are small; otherwise, they are stabilized at an equilibrium. These results are important for understanding the fear effect in food chain systems, prompting us to wonder whether more complex dynamics emerge in food chain systems with quadratic mortality in intermediate predators, and whether more interesting transition phenomena will occur in the fluctuating environment.

Acknowledgments. Sanling Yuan's research is partially supported by National Natural Science Foundation of China (11671260; 12071293). Hao Wang's research is partially supported by Natural Sciences and Engineering Research Council of Canada (Discovery Grant RGPIN-2020-03911 and Accelerator Supplement Grant RGPAS-2020-00090).

Appendix.

Appendix A. The existence of roots of (5). We discuss the positive roots of (5) by considering three cases: $\ell_3^2 < \frac{8}{3}\ell_2\ell_4$, $\ell_3^2 = \frac{8}{3}\ell_2\ell_4$ and $\ell_3^2 > \frac{8}{3}\ell_2\ell_4$.

(1) When $\ell_3^2 < \frac{8}{3}\ell_2\ell_4$, $F_2(u) = 0$ has no positive roots and $F_2(u) > 0$ in $(0, \infty)$ because of $F_2(0) = 2\ell_2 > 0$. This implies that $F_1(u)$ is strictly increasing. Then

(1a) if $\ell_1 \geq 0$, we have $F_1(u) > 0$ in $(0, \infty)$, which indicates that $F(u)$ is an increasing function. It then follows from $\ell_0 < 0$ that $F(u) = 0$ has a unique positive root $u = u^*$.

(1b) if $\ell_1 < 0$, then $F_1(u) = 0$ has a unique positive root $u = \bar{u}$, $F_1(u) < 0$ for $0 < u < \bar{u}$ and $F_1(u) > 0$ for $u > \bar{u}$. We can directly know that $F(u)$ is decreasing in $(0, \bar{u})$ and increasing in (\bar{u}, ∞) . It then follows from $\ell_0 < 0$ that thus $F(u) = 0$ has a unique positive root $u = u^* > \bar{u}$.

(2) When $\ell_3^2 = \frac{8}{3}\ell_2\ell_4$, if $\ell_3 \geq 0$, then $F_2(u) = 0$ has no positive roots. Arguing as above the situation (1), one can obtain that $F(u) = 0$ has a unique positive root; if $\ell_3 < 0$, then $F_2(u) = 0$ has a positive root with multiplicity 2 and $F_2(u) \geq 0$, which means that $F_1(u)$ is an increasing function. Following the same argument as the above situations (1a) and (1b), one can obtain that $F(u) = 0$ has a unique positive root $u = u^*$.

(3) When $\ell_3^2 > \frac{8}{3}\ell_2\ell_4$, then $F_2(u) = 0$ has two roots $u = \beta_1, \beta_2$, where

$$\beta_1 = \frac{-3\ell_3 - \sqrt{9\ell_3^2 - 24\ell_2\ell_4}}{12\ell_4}, \quad \beta_2 = \frac{-3\ell_3 + \sqrt{9\ell_3^2 - 24\ell_2\ell_4}}{12\ell_4}.$$

Then

- (3a) If $\ell_2 < 0$ or $\ell_2 = 0$ and $\ell_3 < 0$, then $F_2(u) = 0$ has a unique positive root $u = \beta_2$. It then follows that $F_1(u)$ is decreasing in $(0, \beta_2)$ and increasing in (β_2, ∞) . Then, when $\ell_1 \leq 0$, one knows that $F(u) = 0$ has a unique positive root $u = u^*$; when $\ell_1 > 0$, there are two cases need to be discussed.
- (3a-1) If $F_1(\beta_2) > 0$, then $F(u)$ is an increasing function and $F(u) = 0$ has a unique positive root $u = u^*$.
- (3a-2) If $F_1(\beta_2) = 0$, further when $F(\beta_2) = 0$, then $u = \beta_2$ is a positive root with multiplicity 3 of $F(u) = 0$; when $F(\beta_2) \neq 0$, $F(u) = 0$ has a unique positive root $u = u^*$.
- (3a-3) If $F_1(\beta_2) < 0$, then $F_1(u) = 0$ has two different roots and we denote them as $u = \gamma_1, \gamma_2$ with $\gamma_1 < \gamma_2$. This implies that $F(u)$ is increasing in $(0, \gamma_1) \cup (\gamma_2, \infty)$ and decreasing in (γ_1, γ_2) . Therefore, when $F(\gamma_1) > 0$ and $F(\gamma_2) < 0$, $F(u) = 0$ has three different positive roots $u = u_1^*, u_2^*$ and u_3^* with $u_1^* < u_2^* < u_3^*$; when $F(\gamma_1) = 0$, u_1^* and u_2^* coincide into a positive root $u = u_{1,2}^* = \gamma_1$, and $F(u) = 0$ has two positive roots $u = u_{1,2}^*, u_3^*$ with $u_{1,2}^* < u_3^*$; when $F(\gamma_1) < 0$, $u_{1,2}^*$ disappears and $F(u) = 0$ has a unique positive root $u = u_3^*$; when $F(\gamma_2) = 0$, u_2^* and u_3^* coincide into a positive root $u = u_{2,3}^* = \gamma_2$, and $F(u) = 0$ has two positive roots $u = u_1^*, u_{2,3}^*$ with $u_1^* < u_{2,3}^*$; when $F(\gamma_2) > 0$, $u_{2,3}^*$ disappears, and $F(u) = 0$ has a unique positive root $u = u_1^*$.
- (3b) If $\ell_2 \geq 0, \ell_3 \geq 0$, then $F_2(u) = 0$ has no positive roots and $F_2(u) > 0$ in $(0, \infty)$ because of $F_2(0) = 2\ell_2 \geq 0$. Therefore, arguing as (1), one can obtain that $F(u) = 0$ has a unique positive root $u = u^*$.
- (3c) If $\ell_2 > 0, \ell_3 < 0$, then $F_2(u) = 0$ has two different positive roots β_1 and β_2 , and $F_1(u)$ is increasing in $(0, \beta_1) \cup (\beta_2, \infty)$ and decreasing in (β_1, β_2) . Then,
- (3c-1) when $\ell_1 < 0$, if $F_1(\beta_1) \leq 0$ or $F_1(\beta_2) \geq 0$, then $F(u) = 0$ has a unique positive root $u = u^*$; if $F_1(\beta_1) > 0$ and $F_1(\beta_2) < 0$, then $F_1(u) = 0$ has three different positive roots and we denote them as $u = \gamma_1, \gamma_2, \gamma_3$ with $\gamma_1 < \gamma_2 < \gamma_3$. It then follows that $F(u)$ is decreasing in $(0, \gamma_1) \cup (\gamma_2, \gamma_3)$ and increasing in $(\gamma_1, \gamma_2) \cup (\gamma_3, \infty)$. Then when $F(\gamma_2) > 0$ and $F(\gamma_3) < 0$, $F(u) = 0$ has three different positive roots $u = u_1^*, u_2^*$ and u_3^* with $u_1^* < u_2^* < u_3^*$; when $F(\gamma_2) = 0$, u_1^* and u_2^* coincide into a positive root $u = u_{1,2}^* = \gamma_2$, and $F(u) = 0$ has two positive roots $u = u_{1,2}^*, u_3^*$ with $u_{1,2}^* < u_3^*$; when $F(\gamma_2) < 0$, $u_{1,2}^*$ disappears and $F(u) = 0$ has a unique positive root $u = u_3^*$; when $F(\gamma_3) = 0$, u_2^* and u_3^* coincide into a positive root $u = u_{2,3}^* = \gamma_3$, and $F(u) = 0$ has two positive roots $u = u_1^*, u_{2,3}^*$ with $u_1^* < u_{2,3}^*$; when $F(\gamma_3) > 0$, $u_{2,3}^*$ disappears, and $F(u) = 0$ has a unique positive root $u = u_1^*$.
- (3c-2) when $\ell_1 \geq 0$, if $F_1(\beta_2) > 0$ or $F_1(\beta_2) = 0$ and $F(\beta_2) \neq 0$, then $F(u) = 0$ has a unique positive root u^* ; if $F_1(\beta_2) = F(\beta_2) = 0$, then $u = \beta_2$ is a positive root with multiplicity 3 of $F(u) = 0$; if $F_1(\beta_2) < 0$, then $F_1(u) = 0$ has two different positive roots and we denote them as $u = \gamma_1, \gamma_2$ with $\gamma_1 < \gamma_2$. It then follows that $F(u)$ is increasing in $(0, \gamma_1) \cup (\gamma_2, \infty)$ and decreasing in (γ_1, γ_2) . Then when $F(\gamma_1) > 0$ and $F(\gamma_2) < 0$, $F(u) = 0$ has three different positive roots $u = u_1^*, u_2^*$ and u_3^* with $u_1^* < u_2^* < u_3^*$; when $F(\gamma_1) = 0$, u_1^* and u_2^* coincide into a positive root $u = u_{1,2}^* = \gamma_1$, and $F(u) = 0$ has two positive roots $u = u_{1,2}^*, u_3^*$ with $u_{1,2}^* < u_3^*$; when $F(\gamma_1) < 0$, $u_{1,2}^*$ disappears and $F(u) = 0$ has a unique positive root $u = u_3^*$; when $F(\gamma_2) = 0$, u_2^* and u_3^* coincide into a

positive root $u_{2,3}^*$, and $F(u) = 0$ has two positive roots $u = u_1^*$, $u_{2,3}^*$ with $u_1^* < u_{2,3}^*$; when $F(\gamma_2) > 0$, $u_{2,3}^*$ disappears, and $F(u) = 0$ has a unique positive root $u = u_1^*$.

Appendix B. The coefficients appearing in (32). The following is the coefficients appearing in (32):

$$\tilde{\alpha}_{00}(\varepsilon) = -\tilde{a}_{00}(\varepsilon)\tilde{b}_{01}(\varepsilon) + \frac{2\tilde{a}_{00}(\varepsilon)\tilde{a}_{02}(\varepsilon)}{\tilde{a}_{01}(\varepsilon)} + \frac{2\tilde{a}_{00}^2(\varepsilon)\tilde{a}_{02}(\varepsilon)\tilde{b}_{01}(\varepsilon)}{\tilde{a}_{01}^2(\varepsilon)} - \frac{2\tilde{a}_{00}^3(\varepsilon)\tilde{a}_{02}(\varepsilon)\tilde{b}_{02}(\varepsilon)}{\tilde{a}_{01}^3(\varepsilon)},$$

$$\begin{aligned} \tilde{\alpha}_{10}(\varepsilon) &= \tilde{a}_{01}(\varepsilon)\tilde{b}_{10}(\varepsilon) - \tilde{a}_{10}(\varepsilon)\tilde{b}_{01}(\varepsilon) - \tilde{a}_{00}(\varepsilon)\tilde{b}_{11}(\varepsilon) - \frac{6\tilde{a}_{00}^2(\varepsilon)\tilde{a}_{02}(\varepsilon)\tilde{b}_{02}(\varepsilon)\tilde{a}_{10}(\varepsilon)}{\tilde{a}_{01}^3(\varepsilon)} \\ &+ \frac{\tilde{a}_{00}(\varepsilon)}{\tilde{a}_{01}(\varepsilon)}(2\tilde{a}_{10}(\varepsilon)\tilde{b}_{02}(\varepsilon) - 2\tilde{a}_{02}(\varepsilon)\tilde{b}_{10}(\varepsilon) - \tilde{a}_{11}(\varepsilon)\tilde{b}_{01}(\varepsilon)) \\ &+ \frac{\tilde{a}_{00}(\varepsilon)}{\tilde{a}_{01}^2(\varepsilon)}\left(4\tilde{a}_{02}(\varepsilon)\tilde{b}_{01}(\varepsilon)\tilde{a}_{10}(\varepsilon) + 2\tilde{a}_{00}(\varepsilon)\tilde{a}_{02}(\varepsilon)\tilde{b}_{11}(\varepsilon) + \tilde{a}_{00}(\varepsilon)\tilde{a}_{11}(\varepsilon)\tilde{b}_{02}(\varepsilon)\right), \end{aligned}$$

$$\begin{aligned} \tilde{\alpha}_{01}(\varepsilon) &= \tilde{a}_{10}(\varepsilon) + \tilde{b}_{10}(\varepsilon) - \frac{\tilde{a}_{00}(\varepsilon)}{\tilde{a}_{01}(\varepsilon)}(\tilde{a}_{11}(\varepsilon) + 2\tilde{b}_{02}(\varepsilon)) - \frac{4\tilde{a}_{02}(\varepsilon)\tilde{a}_{00}(\varepsilon)\tilde{b}_{01}(\varepsilon)}{\tilde{a}_{01}^2(\varepsilon)} \\ &+ \frac{6\tilde{a}_{02}(\varepsilon)\tilde{a}_{00}^2(\varepsilon)\tilde{b}_{02}(\varepsilon)}{\tilde{a}_{01}^3(\varepsilon)}, \end{aligned}$$

$$\begin{aligned} \tilde{\alpha}_{20}(\varepsilon) &= \tilde{a}_{01}(\varepsilon)\tilde{b}_{02}(\varepsilon) - \tilde{a}_{20}(\varepsilon)\tilde{b}_{01}(\varepsilon) - \tilde{a}_{10}(\varepsilon)\tilde{b}_{11}(\varepsilon) + \tilde{a}_{11}(\varepsilon)\tilde{b}_{10}(\varepsilon) \\ &+ \frac{\tilde{a}_{10}^2(\varepsilon)\tilde{b}_{02}(\varepsilon)}{\tilde{a}_{01}(\varepsilon)} + \frac{2\tilde{b}_{02}(\varepsilon)\tilde{a}_{00}(\varepsilon)\tilde{a}_{20}(\varepsilon)}{\tilde{a}_{01}(\varepsilon)} - \frac{2\tilde{a}_{02}(\varepsilon)\tilde{a}_{00}(\varepsilon)\tilde{b}_{20}(\varepsilon)}{\tilde{a}_{01}(\varepsilon)} - \frac{\tilde{a}_{11}(\varepsilon)\tilde{b}_{01}(\varepsilon)\tilde{a}_{10}(\varepsilon)}{\tilde{a}_{01}(\varepsilon)} \\ &- \frac{\tilde{a}_{11}(\varepsilon)\tilde{b}_{11}(\varepsilon)\tilde{a}_{00}(\varepsilon)}{\tilde{a}_{01}(\varepsilon)} - \frac{2\tilde{a}_{02}(\varepsilon)\tilde{a}_{10}(\varepsilon)\tilde{b}_{10}(\varepsilon)}{\tilde{a}_{01}(\varepsilon)} \\ &+ \frac{4\tilde{a}_{02}(\varepsilon)\tilde{a}_{00}(\varepsilon)}{\tilde{a}_{01}^2(\varepsilon)}(\tilde{b}_{01}(\varepsilon)\tilde{a}_{20}(\varepsilon) + \tilde{b}_{11}(\varepsilon)\tilde{a}_{10}(\varepsilon)) \\ &- \frac{6\tilde{a}_{00}(\varepsilon)\tilde{a}_{02}(\varepsilon)\tilde{b}_{02}(\varepsilon)}{\tilde{a}_{01}^3(\varepsilon)}(\tilde{a}_{10}^2(\varepsilon) + \tilde{a}_{00}(\varepsilon)\tilde{a}_{20}(\varepsilon)) \\ &+ \frac{2\tilde{a}_{11}(\varepsilon)\tilde{b}_{02}(\varepsilon)\tilde{a}_{00}(\varepsilon)\tilde{a}_{10}(\varepsilon)}{\tilde{a}_{01}^2(\varepsilon)} + \frac{2\tilde{a}_{02}(\varepsilon)\tilde{a}_{10}^2(\varepsilon)\tilde{b}_{01}(\varepsilon)}{\tilde{a}_{01}^2(\varepsilon)}, \end{aligned}$$

$$\begin{aligned} \tilde{\alpha}_{11}(\varepsilon) &= \tilde{b}_{11}(\varepsilon) + \frac{1}{\tilde{a}_{01}(\varepsilon)}(\tilde{a}_{11}(\varepsilon)\tilde{b}_{01}(\varepsilon) + 2\tilde{a}_{02}(\varepsilon)\tilde{b}_{10}(\varepsilon) - \tilde{a}_{10}(\varepsilon)\tilde{b}_{02}(\varepsilon)) \\ &- \frac{2}{\tilde{a}_{01}^2(\varepsilon)}(\tilde{a}_{11}(\varepsilon)\tilde{a}_{00}(\varepsilon)\tilde{b}_{02}(\varepsilon) - 2\tilde{a}_{02}(\varepsilon)\tilde{a}_{10}(\varepsilon)\tilde{b}_{01}(\varepsilon) - 2\tilde{a}_{02}(\varepsilon)\tilde{a}_{00}(\varepsilon)\tilde{b}_{11}(\varepsilon)) \\ &+ \frac{12\tilde{a}_{02}(\varepsilon)\tilde{a}_{10}(\varepsilon)\tilde{a}_{00}(\varepsilon)\tilde{b}_{02}(\varepsilon)}{\tilde{a}_{01}^3(\varepsilon)}, \end{aligned}$$

$$\tilde{\alpha}_{02}(\varepsilon) = \frac{1}{\tilde{a}_{01}(\varepsilon)}(\tilde{a}_{11}(\varepsilon) + \tilde{b}_{02}(\varepsilon)) + \frac{2\tilde{a}_{02}(\varepsilon)\tilde{b}_{01}(\varepsilon)}{\tilde{a}_{01}^2(\varepsilon)} - \frac{6\tilde{a}_{02}(\varepsilon)\tilde{a}_{00}(\varepsilon)\tilde{b}_{02}(\varepsilon)}{\tilde{a}_{01}^3(\varepsilon)}$$

Appendix C. Stochastic sensitivity analysis. We first show the sensitivity analysis for the equilibrium. Define

$$W = \begin{pmatrix} w_{11} & w_{12} \\ w_{21} & w_{22} \end{pmatrix}$$

be the stochastic sensitivity matrix of any equilibrium (u^*, v^*) . It follows from [31] that W satisfies

$$\begin{aligned} 2J_{11}w_{11} + J_{12}w_{12} + J_{12}w_{21} &= -g_{11}^2, \\ J_{21}w_{11} + (J_{11} + J_{22})w_{12} + J_{12}w_{22} &= 0, \\ J_{21}w_{11} + (J_{11} + J_{22})w_{21} + J_{12}w_{22} &= 0, \\ J_{21}w_{12} + J_{21}w_{21} + 2J_{22}w_{22} &= -g_{22}^2, \end{aligned}$$

where $g_{11} = u^*$, $g_{22} = v^*$, $J_{i,j}(i, j = 1, 2)$ is defined by (7) and stands for the elements of Jacobi matrix evaluated at (u^*, v^*) . Then the confidence ellipse equation can be written as

$$\langle (u - u^*, v - v^*)^T, W^{-1}(u - u^*, v - v^*)^T \rangle = -2\sigma^2 \ln(1 - P),$$

where P is the fiducial probability.

In what follows, we compute the stochastic sensitivity functions of the limit cycle. For convenience, we define

$$\begin{aligned} F_1(u, v) &= \frac{ru}{1 + kv} - du - au^2 - \frac{puv}{1 + cu}, \\ F_2(u, v) &= -mv^2 + \frac{quv}{1 + cu}, \end{aligned}$$

and denote this limit cycle mentioned as above as $\mathcal{T}(u(t), v(t))$, $t \in [0, T]$, where T is the period.

According to [31], we know that the stochastic sensitivity functions $\vartheta(t)$ of $\mathcal{T}(u(t), v(t))$ satisfies

$$\begin{aligned} \frac{d\vartheta(t)}{dt} &= m(t)\vartheta(t) + n(t), \\ \vartheta(0) &= \vartheta(T), \end{aligned}$$

where

$$\begin{aligned} m(t) &= 2j_{11}(t)g_1^2(t) + 2(j_{12}(t) + j_{21}(t))g_1(t)g_2(t) + 2j_{22}(t)g_2^2(t), \\ n(t) &= s_{11}(t)g_1^2(t) + s_{22}(t)g_2^2(t), \end{aligned}$$

where $J_{ij}(i, j = 1, 2)$ is evaluated at \mathcal{T} , $s_{11}(t) = u^2|_{\mathcal{T}}$, $s_{22}(t) = v^2|_{\mathcal{T}}$, and

$$\begin{aligned} g_1(t) &= \frac{F_2(u, v)}{\sqrt{F_1^2(u, v) + F_2^2(u, v)}} \Big|_{\mathcal{T}}, \\ g_2(t) &= -\frac{F_1(u, v)}{\sqrt{F_1^2(u, v) + F_2^2(u, v)}} \Big|_{\mathcal{T}}. \end{aligned}$$

Then the boundaries $\mathcal{T}_{1,2}(t)$, $t \in [0, T]$, of the confidence bands with the fiducial probability $P = 0.95$ are

$$\begin{aligned} \mathcal{T}_1(t) &= \mathcal{T}(t) + 1.9597\sigma\sqrt{\vartheta(t)}g(t), \\ \mathcal{T}_2(t) &= \mathcal{T}(t) - 1.9597\sigma\sqrt{\vartheta(t)}g(t), \end{aligned} \tag{44}$$

where $g(t) = (g_1(t), g_2(t))^T$.

REFERENCES

- [1] I. Bashkirtseva and L. Ryashko, [Sensitivity analysis of stochastic attractors and noise-induced transitions for population model with allee effect](#), *Chaos*, **21** (2011), 047514.
- [2] I. Bashkirtseva, L. Ryashko and I. Tsvetkov, [Sensitivity analysis of stochastic equilibria and cycles for the discrete dynamic systems](#), *Dynamics of Continuous, Discrete and Impulsive Systems, Series A: Mathematical Analysis*, **17** (2010), 501-515.
- [3] P. Chesson and J. J. Kuang, [The interaction between predation and competition](#), *Nature*, **456** (2008), 235-238.
- [4] M. Clinchy, M. J. Sheriff, L. Y. Zanette and R. Boonstra, [Predator-induced stress and the ecology of fear](#), *Funct. Ecol.*, **27** (2013), 56-65.
- [5] P. Cong, M. Fan and X. Zou, [Dynamics of a three-species food chain model with fear effect](#), *Commun. Nonlinear Sci. Numer. Simul.*, **99** (2021), 105809.
- [6] S. Creel and D. Christianson, [Relationships between direct predation and risk effects](#), *Trends Ecol. Evol.*, **23** (2008), 194-201.
- [7] B. K. Das, D. Sahoo and G. Samanta, [Impact of fear in a delay-induced predator-prey system with intraspecific competition within predator species](#), *Math. Comput. Simulat.*, **191** (2022), 134-156.
- [8] E. A. Fulton, A. D. Smith and C. R. Johnson, [Mortality and predation in ecosystem models: Is it important how these are expressed?](#), *Ecol. Model.*, **169** (2003), 157-178.
- [9] M. Hossain, N. Pal, S. Samanta and J. Chattopadhyay, [Fear induced stabilization in an intraguild predation model](#), *Int. J. Bifurcat. Chaos*, **30** (2020), 2050053.
- [10] L. Imhof and S. Walcher, [Exclusion and persistence in deterministic and stochastic chemostat models](#), *J. Differ. Equations*, **217** (2005), 26-53.
- [11] A. Li and X. Zou, [Evolution and adaptation of anti-predation response of prey in a two-patchy environment](#), *Bull. Math. Biol.*, **83** (2021), Paper No. 59, 27 pp.
- [12] D. J. S. Montagnes, X. Zhu, L. Gu, Y. Sun, J. Wang, R. Horner and Z. Yang, [False exclusion: A case to embed predator performance in classical population models](#), *Am. Nat.*, **194** (2019), 654-670.
- [13] E. H. Nelson, C. E. Matthews and J. A. Rosenheim, [Predators reduce prey population growth by inducing changes in prey behavior](#), *Ecology*, **85** (2004), 1853-1858.
- [14] S. Pal, N. Pal, S. Samanta and J. Chattopadhyay, [Fear effect in prey and hunting cooperation among predators in a leslie-gower model](#), *Math. Biosci. Eng.*, **16** (2019), 5146-5179.
- [15] P. Panday, N. Pal, S. Samanta and J. Chattopadhyay, [Stability and bifurcation analysis of a three-species food chain model with fear](#), *Int. J. Bifurcat. Chaos*, **28** (2018), 1850009.
- [16] K. L. Pangle, S. D. Peacor and O. E. Johannsson, [Large nonlethal effects of an invasive invertebrate predator on zooplankton population growth rate](#), *Ecology*, **88** (2007), 402-412.
- [17] L. Perko, *Differential Equations and Dynamical Systems*, Springer, New York, 1996.
- [18] E. L. Preisser, D. I. Bolnick and M. F. Benard, [Scared to death? the effects of intimidation and consumption in predator-prey interactions](#), *Ecology*, **86** (2005), 501-509.
- [19] T. Qiao, Y. Cai, S. Fu and W. Wang, [Stability and hopf bifurcation in a predator-prey model with the cost of anti-predator behaviors](#), *Int. J. Bifurcat. Chaos*, **29** (2019), 1950185.
- [20] S. Rana, A. R. Bhowmick and T. Sardar, [Invasive dynamics for a predator-prey system with allee effect in both populations and a special emphasis on predator mortality](#), *Chaos*, **31** (2021), 033150.
- [21] S. K. Sasmal and Y. Takeuchi, [Dynamics of a predator-prey system with fear and group defense](#), *J. Math. Anal. Appl.*, **481** (2020), 123471.
- [22] C. Shan, Y. Yi and H. Zhu, [Nilpotent singularities and dynamics in an sir type of compartmental model with hospital resources](#), *J. Differ. Equations*, **260** (2016), 4339-4365.
- [23] C. Wang, S. Yuan and H. Wang, [Spatiotemporal patterns of a diffusive prey-predator model with spatial memory and pregnancy period in an intimidatory environment](#), *J. Math. Biol.*, **84** (2022), Paper No. 12, 36 pp.
- [24] H. Wang and Y. Kuang, [Alternative models for cyclic lemming dynamics](#), *Math. Biosci. Eng.*, **4** (2007), 85-99.
- [25] X. Wang, Y. Tan, Y. Cai and W. Wang, [Impact of the fear effect on the stability and bifurcation of a leslie-gower predator-prey model](#), *Int. J. Bifurcat. Chaos*, **30** (2020), 2050210.
- [26] X. Wang, L. Zanette and X. Zou, [Modelling the fear effect in predator-prey interactions](#), *J. Math. Biol.*, **73** (2016), 1179-1204.

- [27] X. Wang and X. Zou, [Pattern formation of a predator-prey model with the cost of anti-predator behaviors](#), *Math. Biosci. Eng.*, **15** (2018), 775-805.
- [28] Y. Wang and X. Zou, [On a predator-prey system with digestion delay and anti-predation strategy](#), *J. Nonlinear Sci.*, **30** (2020), 1579-1605.
- [29] Y. Xia and S. Yuan, [Survival analysis of a stochastic predator-prey model with prey refuge and fear effect](#), *J Biol. Dynam.*, **14** (2020), 871-892.
- [30] A. Yang, B. Song and S. Yuan, [Noise-induced transitions in a non-smooth sis epidemic model with media alert](#), *Math. Biosci. Eng.*, **18** (2021), 745-763.
- [31] S. Yuan, D. Wu, G. Lan and H. Wang, [Noise-induced transitions in a nonsmooth producer-grazer model with stoichiometric constraints](#), *Bull Math Biol.*, **82** (2020), Paper No. 55, 22 pp.
- [32] L. Zanette, A. F. White, M. C. Allen and M. Clinchy, [Perceived predation risk reduces the number of offspring songbirds produce per year](#), *Science*, **334** (2011), 1398-1401.
- [33] L. Y. Zanette and M. Clinchy, [Ecology of fear](#), *Curr. Biol.*, **29** (2019), 309-313.
- [34] H. Zhang, Y. Cai, S. Fu and W. Wang, [Impact of the fear effect in a prey-predator model incorporating a prey refuge](#), *Appl. Math. Comput.*, **356** (2019), 328-337.
- [35] S. Zhang, S. Yuan and T. Zhang, [A predator-prey model with different response functions to juvenile and adult prey in deterministic and stochastic environments](#), *Appl. Math. Comput.*, **413** (2022), Paper No. 126598, 26 pp.
- [36] S. Zhang, T. Zhang and S. Yuan, [Dynamics of a stochastic predator-prey model with habitat complexity and prey aggregation](#), *Ecol. Complex.*, **45** (2021), 100889.

Received June 2022; revised November 2022; early access December 2022.